Energy LAB

REVIEW ARTICLE

Energy Lab 2022, 1, 220011

Towards the intercalation and lithium plating mechanism for high safety and fast-charging lithium-ion batteries: a review

Yi Yang[1,2], Lei Xu[1,2], Chong Yan[1,2*], Jiaqi Huang[1,2] and Qiang Zhang[3*]

The ever-increasing demand of portable electronics and electric vehicles has consistently promoted the development of lithium-ion batteries (LIBs) in the direction of higher energy density, higher safety, and faster charging. However, present high-energy LIBs are insufficient to sustain extra-fast power input without adverse consequences, which is mainly affected by the lithium (Li) plating on graphite electrode. The goal of this review is to enable graphite anode to support higher current and improve safety by ameliorating undesired Li plating from fundamentals and detections. Hence, the interaction, containing solid electrolyte interphase formation, Li^+ intercalation/plating behavior, between graphite and Li^+ be discussed in depth. Besides, the cognitive process of Li^+ intercalation/plating kinetics as well as the inner mechanisms of Li plating especially in 3 extreme conditions (high state-of-charge, high charging-rate, and low temperature) are highly desirable to investigate Li plating comprehensively.

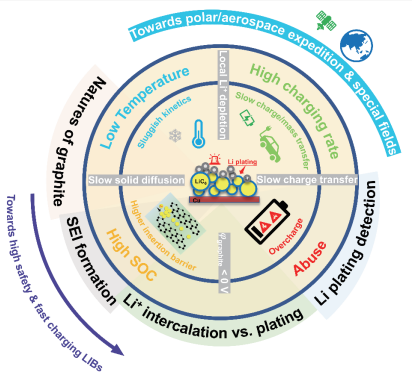

Meanwhile, issues induced by Li plating, detection methods of Li deposition and knowledge gaps are identified for the follow-up research directions of Li plating in LIBs.

The invention of the battery gave humans the ability to store and release electric charges. Retrospect the development of commercial batteries[1]: The lead/acid battery was invented in 1859 by Planté and developed further by Faure in 1881. A lead/acid battery consists of lead, lead oxide and sulfuric acid, whose voltage can reach about 2 V. Due to the low cost and the stability of recycling, lead/acid battery still has the overwhelming share of the consumer battery market, despite it has been invented more than 160 years. Nickel/cadmium battery is another most widely utilized after the lead/acid battery, which has better cycling performance than that of lead/acid battery both at ambient and low temperature. However, due to the high cost of nickel/cadmium battery and its memory effect as well as environmental pollution problems, it was gradually replaced by the nickel-metal hydride battery developed later. New battery systems are constantly being developed, which gradually develop toward portable, low cost, high energy density and high safety, etc. As the protagonist of the story, the lithium battery is moving forward step by step. From its birth to the large-scale use of today, there are numerous great minds make huge efforts for it.[2]

At 1913, lithium (Li) metal was discovered to own the lowest electrode potential (−3.04 V).[3] Then, the novel concept of intercalation reaction in layered oxide cathode material titanium disulfide (TiS_2)[4] and lithium cobaltite (LCO, short for $LiCoO_2$)[5] was suggested, which can allow reversible intercalation/de-intercalation of lithium-ions (Li^+). Until to the replacement of dangerous lithium anode with graphite as anode material, the lithium-ion batteries (LIBs), as one of the greatest inventions in history, have profoundly reshaped our lifestyles after the commercialization in 1991, due to high energy density, long lifespan, and reliable safety.[2,6–11] Recently, the ever-increasing portable electronics, electric vehicles (EVs), and large-scale energy storage constantly promote the development of LIBs towards higher energy density, faster charging, and lower cost.[12–17]

Especially in the field of EVs, despite the fact that EVs have achieved good development in various technologies and low cost in recent years, there is still a lack of consumer acceptance. Hence, the current market acceptance of EVs is relatively low. One of the key reasons is that the fast-charging capacity of LIBs in EVs is insufficient, so that recharging the EVs

[1] *School of Materials Science and Engineering, Beijing Institute of Technology, Beijing 100081, China*

[2] *Advanced Research Institute of Multidisciplinary Science, Beijing Institute of Technology, Beijing 100081, China*

[3] *Beijing Key Laboratory of Green Chemical Reaction Engineering and Technology, Department of Chemical Engineering, Tsinghua University, Beijing 100084, China*

* Corresponding author, E-mail: yanc@bit.edu.cn; zhang-qiang@mails.tsinghua.edu.cn

Received $articlereceiveddate; Accepted ; Published online

© 2022 The Author(s). *Energy Lab* published by Lab Academic Press

DOI: 10.54227/elab.20220011

will take considerably longer than refuelling internal combustion engine (ICE) cars. Therefore, improving the fast-charging capacity of LIBs will be a powerful force to satisfy the needs of the society and push electric vehicles to the market.

Many organizations have proposed different fast charging goals, such as the extreme fast charging (XFC) proposed by the US Department of Energy, which aims to facilitate the charging experience of battery electric vehicles (BEVs) to catch up with that of refuelling ICE cars in 3-5 minutes.[18,19] Further, the US Advanced Battery Consortium (USABC) targets high-performance batteries for EVs applications to obtain 80% state of charge (SOC) within 15 minutes, and the available system energy is 45 kWh with 1000 available energy dynamic stress test cycles.[19]

However, it is still difficult to achieve the targets of fast charging. Many studies have pointed out that the key to limiting fast charging capacity lies in the battery itself, especially the anode of a battery.[20] The battery will inevitably endure a larger current under high rate charging in order to save time. Although the charging time saved, the battery will suffer more significant effect. Specifically, high-rate charging will trigger a series of side reactions, such as Li plating, mechanical effects, and heat generation, which are the culprits that accelerate batteries aging and even cause uncontrollable safety issues of the battery.[19]

When it comes to the application of LIBs, it is still challenging for LIBs adoption in cold regions at high latitudes/altitudes and special application (e.g., polar/aerospace expedition and military fields). In these areas or applications, batteries are required to work well below −20° C, or even below −60° C.[21] However, the optimal working temperature of LIBs should be controlled in 15–35° C. Low temperatures restrict the charging/discharging rate severely, resulting from the sluggish kinetics in mass transfer and interfacial charge transfer process. Further, the larger polarization generating by untoward kinetics processes under low temperature is much more favorable for Li plating on graphite compared to the normal intercalation behavior.

The abuse of electricity and heat are the key cause of battery thermal runaway. The safety performance and thermal stability of the battery will be decreased due to the abuse of electricity.[22–24] The side reaction between the plated Li metal and electrolyte is the main reason for the decrement of the thermal stability of the battery during overcharge.[23] Meanwhile, separator can be punctured by plated Li, resulting in a local short circuit which will facilitate the battery thermal runaway. Considering that Li plating plays a decisive role in worsening the safety performance and fast charging capacity of LIBs, it is very important to study the mechanism of Li plating and monitor its occurrence.

To be specific, the term "Li plating" commonly refers to the metallic Li deposition on the graphite electrode. The thermodynamic potential of LiC_6 which is the stage1 of GICs (short for graphite intercalation compounds) of Li in graphite is very close to that of Li metal (0 V vs. Li/Li^+). Li metal can be easily deposited on graphite particles, especially under the conditions of high charging rate, high state of charge, low temperature and abuse (see Figure 1).[25–29] Further, the plated dendritic Li will lead to the loss of active Li or induce the internal short circuit, increasing the resistance of the battery and even causing safety problems.[19,30,31]

There have been many studies of Li plating, but there are few reports about the research journey of Li plating and the analysis related to the structure and interface chemistry of graphite. Herein, we introduce the structure and interface chemistry of graphite and also comb the researchers' cognition of Li intercalation and plating. Firstly, this review introduces the structure nature of graphite which is favourable for Li reversible intercalation and de-intercalation. Secondly, the process of Li intercalated into graphite with/without the electrolyte is reviewed respectively. It should be noted that the electrode/electrolyte interphase (EEI) will be formed during the first cycle of charging and discharging process, which has a great impact on the insertion and plating of Li^+. Hence, it is vital to explore the SEI formation, composition and structure. During SEI formation, the insertion of Li^+ into graphite is also

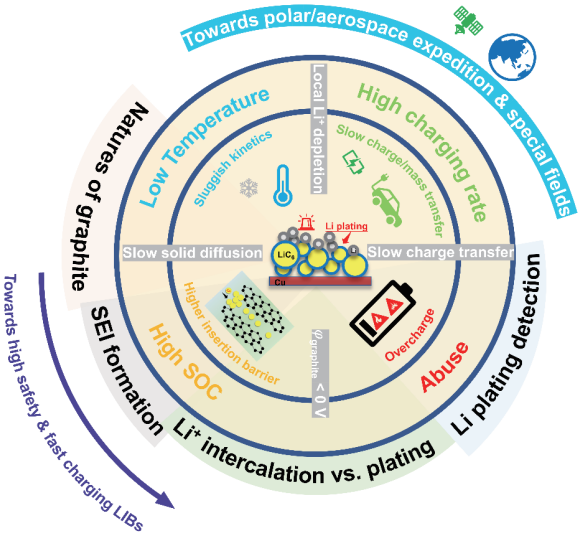

Fig. 1 Schematic drawing of lithium plating on graphite electrode.

DOI: 10.54227/elab.20220011

taking place. The intercalation process of Li into graphite is also introduced in detail, the factors limiting the intercalation of Li^+ are discussed as well. In the following, the research process of Li intercalation kinetics and Li plating is reviewed, and then 4 important mechanisms affecting Li plating are discussed. Further, the mechanism of Li deposition is analysed in detail under the extreme conditions of LIBs (high charging-rate, low temperature, and high state-of-charge). This article also analyses the adverse effect caused by Li plating and detection method of Li plating in order to predict the onset of Li deposition. Finally, the prospect of follow-up research directions on Li plating in LIBs is also presented.

What do we know about graphite?

It is well acknowledged that the operating potential of the graphite anode (~0.1 V vs. Li/Li^+) is above 0 V in terms of thermodynamics. And graphite has the high theoretical specific capacity of 372 mAh g^{-1} so that the graphite is still by far the most commonly used commercial anode material for LIBs.[32,33] As depicted in Figure 2a, graphite has a typical layered structure and each layer is composed of carbon atoms.[34] The carbon atoms in the layer are sp^2 hybridized to form a covalent bond, so that each carbon atom can be connected to three adjacent carbon atoms at an angle of 120° in the same the plane. The chemical bonds are cross-linked and extended, hence, the six carbon atoms form a regular hexagonal carbon ring. The carbon ring expands on the plane to form a graphite sheet structure. At the same time, the remaining unhybridized *p*-orbitals of each carbon atom interact with electrons to form π bonds, allowing electrons to move freely between graphite layers. Thus, graphite has good electrical conductivity. Due to π electrons which can absorb visible light, the graphite has a black coloration. Because the carbon atoms between the same carbon layers are covalently bonded, it is difficult to destroy them. However, in the vertical direction, the distance between the two layers is 3.354 Å, which is more than twice of the gap between two carbon atoms in plane layer. Because the two adjacent carbon layers are combined with weak van der Waals forces. This layered structure can allow foreign chemical substances, (such as certain atoms, molecules, ions or complex ions and so on), smoothly embedding without destroying the graphite network structure in the carbon layer to form GICs (short for graphite intercalation compound).[35,36] Those substances inserted between the graphite layers are called guest, and graphite acts as the host. The reaction of the guest embedded in the graphite host is called the intercalation reaction. Although there are two different layer stacking order in 2H and 3R graphite phases, the intercalation mechanism and capacities of the two graphite phases are similar.[37]

It is important to highlight the interaction of Li^+ with graphite, especially the state of inserted Li in the graphite layers. Graphite undergoes a series of phase transitions as the insertion of Li. Various phases, also referred to as stages, are defined according to the Li concentration in graphite. The in-

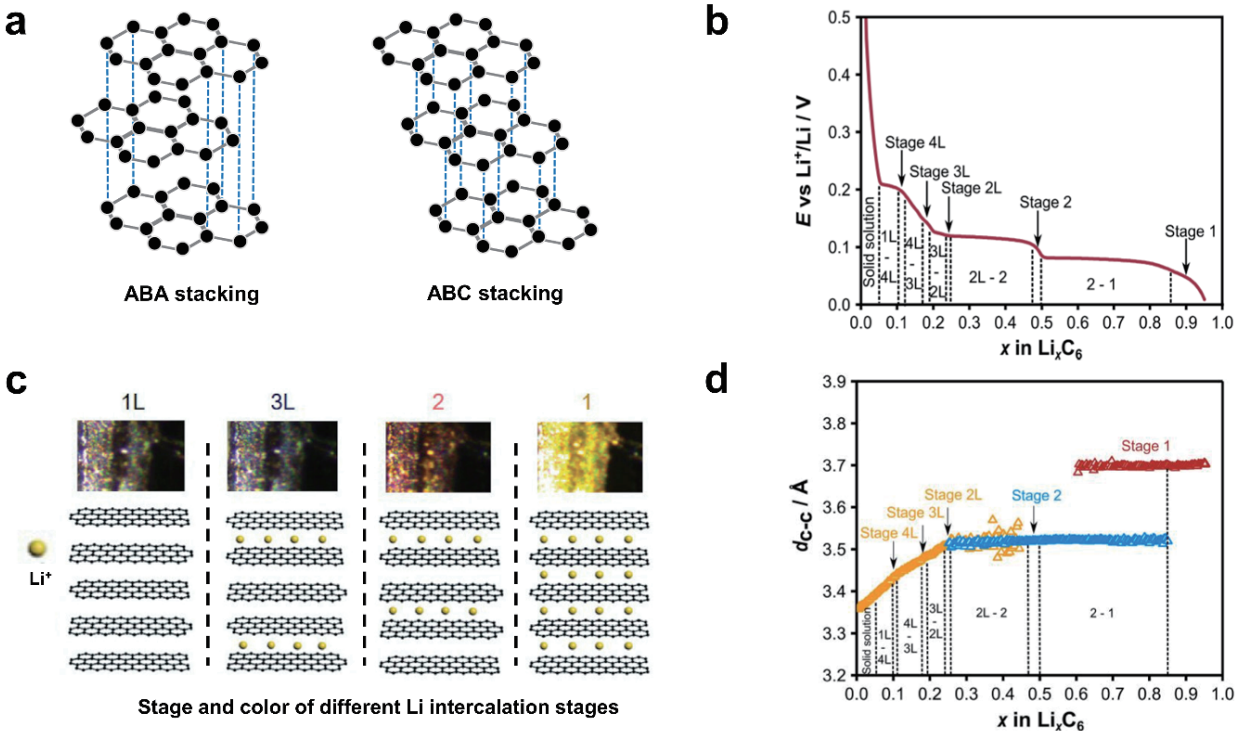

Fig. 2 **a** Schematic of the graphite structure with two different stacking sequences including ABAB (2H) and ABCABC (3R). And ABA stacking is the main types of graphite. **b** The different lithium intercalation stages and phase transition regimes in the second cycle.[38] Copyright 2018, American Chemical Society. **c** The colour and structure of stages 1L, 3L, 2, 1.[51] Copyright 2021, Elsevier. **d** Rietveld refinement results for the second cycle: interlayer spacing d_{C-C} vs. lithium content.[38] Copyright 2018, American Chemical Society.

DOI: 10.54227/elab.20220011

tercalation of Li is assumed to have no in-plane order if the x(Li) < 0.25 in Li_xC_6, which is the dilute region of stages 1L, 4L, 3L and 2L. Phases that are present at higher degrees of lithiation, such as stage 2 and stage 1 (LiC_{12} and LiC_6 respectively) are assigned to space group *P*6/mmm, which corresponding to the stacking of graphene layers shifts from AB sequence to AA sequence.[38] The different Li intercalation stages and phase transition regimes are exhibited in Figure 2b. It was demonstrated in a number of studies that the number in terms of each stage (included the stages 1L, 4L, 3L, 2L, 2, and 1) are referred to the number of unoccupied graphene layers between two occupied layers. The colour and structure of stages 1L, 3L, 2, 1 are depicted in Figure 2c. A 13.2% total volume expansion is obtained when the C_6 is fully lithiated to LiC_6 by using the *operando* X-ray diffraction (XRD) and electrochemical testing.[38] Another interesting finding is that there is a quasi linear behaviour of the interlayer spacing $d_{C\text{-}C}$ from the C to stage 2L transformation, however, the interlayer spacing is rarely changed during the 2L to 2 transformation. And a notable increment of $d_{C\text{-}C}$ can be seen in stage 1, due to the intercalated Li in each graphene layer. And the interlayer distance between adjacent graphene layers increases with ~10% when Li and graphite form LiC_6 (see Figure 2d).

What do we know about the process of Li intercalated into graphite?

The interaction between Li and graphite

The diffusion of adsorbed Li on the surface of a graphite single crystal was reported by Surf. Sci. methods.[39,40] It was found that adsorbed Li atoms are mobile on the graphite surface, even at temperatures as low as −173 °C.[40] Furthermore, it was reported that the sub-monolayers of Li are disordered so that the Li dendrite can grow easily. Jäckle and Groβ went one step further and studied adsorbed Li atoms on a Li (001) surface via *ab-initio* calculations, which mimicked the situation when several atomic layers of Li have already been deposited on a graphite surface.[41] And they attributed the dendritic growth of Li to the rather weak interaction of neighbouring adsorbed Li atoms and the diffusion properties of Li on the Li (001) surface, which is favourable for unsmooth Li growth on graphite surface and metal Li surface. Besides, there is another research about the process of chemical intercalation of Li into a HOPG single crystal by utilizing evaporation Li atoms onto the surface of a HOPG in ultra-high vacuum. It was reported that sub-monolayer coverages of Li diffuse into graphite with an activation barrier of only 0.16 ± 0.02 eV by monitoring the surface coverage by Auger electron spectroscopy (AES) and surface-dependent chemical reaction.[42] Recently, an *operando* Raman spectroscopy measurement was carried out to investigate the layer breathing modes in lithiated graphite, which gets detailed empirical evidence of Li intercalation/de-intercalation into graphite. By using *operando* measurements, LiC_{18}, LiC_{12}, and LiC_6 phases are observed via distinct low-frequency Raman features, which are caused by the displacement of the graphite lattice by induced local strain. What is more, the new findings indicate graphene-like characteristics in the lithiated graphite under the deep charged condition due to the imposed strain by the intercalated Li.[35]

Although the above study only considered the reaction between Li and graphite without the existence of electrolyte, it also provided a train of thought for studying the kinetic process of Li^+ inserted in graphite. It was also proposed that the process of Li^+ intercalated into graphite proceeds in the form of shrinking core because the graphite particle do not have enough time to reach equilibrium.[43]

A remarkable finding is that the intercalation process is more inclined on the edge plane of graphite rather than the basal plane, because the energy barriers for de-solvation and moving Li^+ into the graphite lattice are in the range of 0.3–0.7 eV for the edge plane while they are ~10 eV for the basal plane.[44–49] Although Yao et al.[50] reported that the energy barrier through the basal plane can be decreased to 6.35–2.36 eV with different defects, it is still an order of magnitude higher compared to the barrier for diffusion through the edge plane. Thus, it is important to highlight that Li^+ intercalation into graphite through the edge plane is much more likely compared to the basal plane. Gao et al.[51] studied the Li insertion process utilizing a single graphite particle by the in-situ optical microscopy, and found that the phase transformation of Li intercalation into graphite was carried out in the way of shrinking core. Another surprising finding is that the edge plane of the graphite particle first changes colour and then moves inward, which is in well consistent with that Li^+ are more likely to diffuse through the edge plane of the graphite. Meanwhile, it is also observed that metallic Li deposits on the edge plane of the graphite first.

Charging process of graphite anodes

SEI: formation, composition and structure

In the charging stage of LIBs, Li^+ escapes from the cathode and reaches the anode through the electrolyte and separator. At the same time, the potential of cathode increases together with the decrease of anode potential, and the voltage of full battery lifts. In the discharge process of the battery, Li^+ returns from the anode to the cathode, reducing the voltage of the battery. With the increase/decrease of the potential in the battery, the electrochemical reaction also takes place between the electrolyte and the electrode, and the solid phase oxidation/reduction products pile up to form an interface film. The stability of the interface film is vitally important for the cycle performance of the battery.[52] On the one hand, part of Li^+ will be consumed during the formation of the interface film, resulting in the loss of battery capacity. On the other hand, the interfacial film has the properties of ion conduction and electronic insulation, which can guarantee the rapid migration of Li^+ and prevent the continuous decomposition of electrolyte components, as well as preventing the irreversible destruction of electrode materials caused by the co-intercalating of solvent molecules.[53]

It should be pointed that the interface film can be unified as the electrode/electrolyte interphase (EEI), and the film that forms on the surface of the anode is commonly known as the solid electrolyte interphase (SEI).[54] For graphite anode, with the decrease of surface potential, a variety of components (cation, solvent, anion, electrolyte additive, trace water) on the surface of the electrode competitive reaction, and reduction to produce SEI. The order and rate of reduction reaction

DOI: 10.54227/elab.20220011

depends on the reduction potential, concentration, reaction activation energy and other factors of each component. An et al.[55] introduced that the SEI formation potential range on the graphite surface was between 0.8 and 0.2 V (vs. Li/Li$^+$), and the organic/inorganic insoluble products produced by reduction reaction were deposited on the surface of graphite anode, while the soluble products diffused into the electrolyte (Figure 3a). If the SEI is not fully formed, and the graphite anode potential continues to drop below 0.2 V (vs Li/Li$^+$), the solvent molecules and the solvation groups around Li$^+$ will co-inserted between the graphite layers. If too much co-intercalation occurs, the graphite layer will be exfoliated, causing irreversible loss to the stability of the graphite anode.

Liu et al.[56] used electrochemical quartz crystal microbalance (EQCM), differential electrochemical mass spectrometer (DEMS) and atomic force microscopy (AFM) to monitor the formation process of SEI on the surface of HOPG. As shown in Figure 3b and 3c, cyclic voltammetry (CV) was used to scan from open circuit potential (3.0 V vs. Li/Li$^+$) to 0.0 V (sweep rate 1.0 mV s^{-1}), and the formation process of SEI was divided into four stages.

(1) When the voltage drops from 2.0 V to 0.91 V, irregular island deposition can be found on the graphite surface at this stage, corresponding to the formation of LiF, which can occur in either a chemical or an electrochemical way.

(2) At the stage of 0.91 V to 0.74 V, the solvent molecules and the solvation structure formed by Li$^+$ co-intercalated into the graphite layers.

(3) In the stage from 0.74 V to 0 V, the ethylene carbonate (EC) in the initial solvation sheath co-intercalated in the graphite begins to reduce, and the deposited particles on the graphite begin to increase and aggregate in large quantities, which can be ascribed to a well-developed SEI formation mainly consisting of lithium ethylene di-carbonate (LEDC).

(4) In the subsequent forward sweep stage, when the voltage rises to more than 0.3 V, some organic components in the SEI undergo re-oxidation.

Considerable research efforts have been devoted to the main component of the SEI in initial stage, which is proven to the simple LiF and LEDC.[57–59] However, the product in the initial SEI is extremely complicated due to that the initial SEI can evolve into an extremely intricate mixture of compounds during repeated cycling. There are mainly 2 reasons for such intricacy originates. The first reason is the instability of initial SEI in terms of the chemical component and structure.[57] Specifically, LEDC which is considered to be the initial component of SEI from the reduction of EC can be re-oxidated. Notably, it should be pointed that lithium ethylene mono-carbonate (LEMC), instead of LEDC, was proved to be the major SEI ingredient, since the LEMC has higher ionic conductivity compared to the ionic insulated LEDC.[60] Secondly, the SEI is chemically sensitive to various destroyers in its surroundings.[61,62] For instance, the dissolution of transition metal ions from cathode, carbon dioxide generated from solvent oxidation could alter the structure and composition of the SEI, which leads to the complicated compounds in the SEI, such as lithium fluorophosphates, lithium carboxylates, polyethylene oxides, Li_2O, LiF, and so on.

When it comes to the structural model of the SEI, people began to pay attention to the structure and composition of

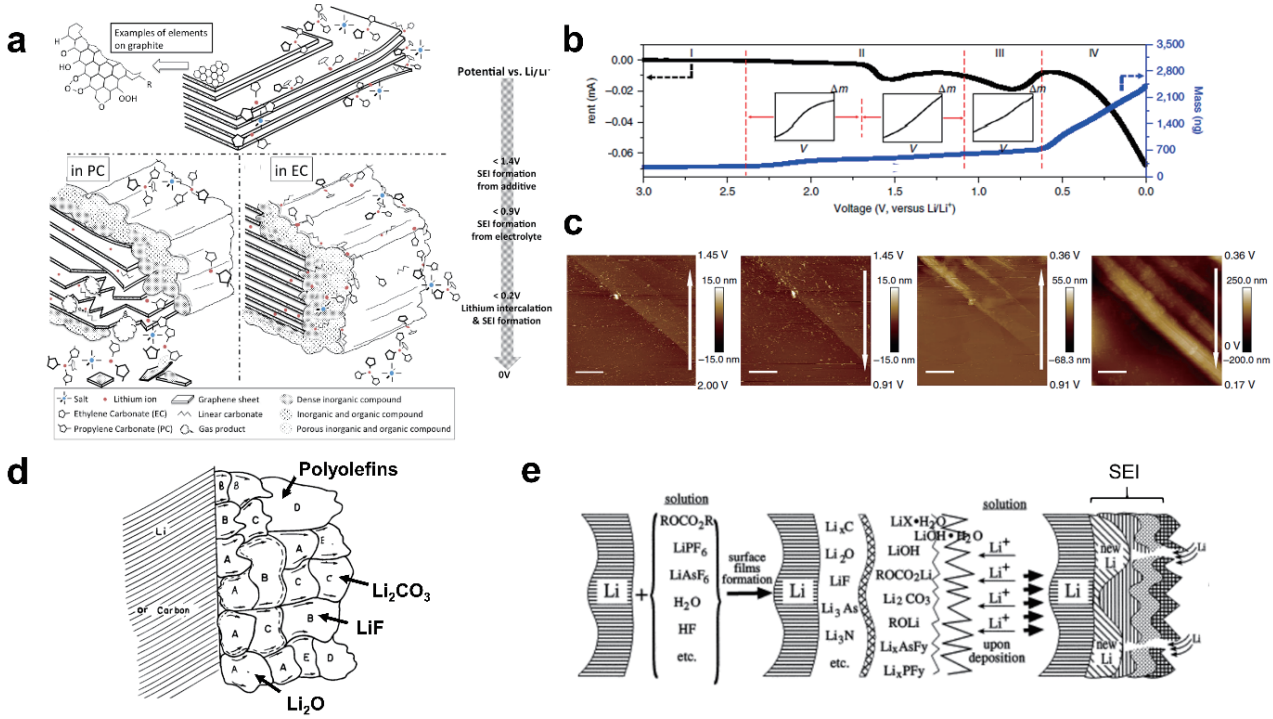

Fig. 3 **a** Schematic of the SEI formation process on graphite surface.[55] Copyright 2016, Elsevier. **b** Curve of potential and mass change during the formation of SEI on graphite surface.[56] Copyright 2018, Springer Nature. **c** In-situ AFM image of graphite cathode surface during potential change.[56] Copyright 2018, Springer Nature. **d** The traditional mosaic model to describe the SEI with multiple organic/inorganic components.[65] Copyright 1997, IOP Publishing. **e** Schematic diagram of SEI layered structure model.[66] Copyright 2000, Elsevier.

DOI: 10.54227/elab.20220011

the membrane on the anode surface since 1970.[63] In 1977, Dey et al.[64] tried to characterize the substances formed on the surface of lithium. Since 1990, the concept of SEI has been extended from lithium metal anode to graphite anode. In 1997, Peled et al.[65] proposed the mosaic model of SEI. And then, Aurbach et al.[66] proposed the layered model of SEI in 1999. Mosaic model and layered model are two main models used to describe SEI.

In the Mosaic SEI, the organic and inorganic products generated by the reduction of electrolyte components are randomly distributed on the electrode surface,[67,68] as depicted in Figure 3d. However, the formation of heterogeneous mosaic structure will affect the transmission path of Li^+, because Li^+ always migrates along the channel with higher migration rate.[63] Due to the different migration rate along the abundant components of the SEI, it is difficult to realize the homogenization intercalation/de-intercalation process of Li^+, so that it will cause dendritic Li and dead Li. For the layered model of SEI, the reduction products of electrolyte components are uniformly distributed on the electrode surface to form a layered structure[69], as shown in Figure 3e. Generally, it is composed of inorganic inner layer with low oxidation state (such as LiF, Li_2O Li_2CO_3, LiOH, etc.) and organic outer layer with high oxidation state (such as $ROCO_2Li$, ROLi, etc.). In the initial formation stage of SEI, the electrolyte components are firstly reduced to organic products, and the components closer to the electrode surface are later reduced to relatively stable inorganic substances, which greatly affects the electronic insulation performance of SEI.[63,69–71]

With the help of analytical instruments, the evolution process of the EEI can be monitored through the feedback of signals. But to explore the formation mechanism of the EEI needs to be explained from a more microscopic perspective. Recent studies have found that the initial structure of EDL (electric double layer) had a greater influence on the formation, namely the inner Helmholtz layer specific adsorption of Li^+ and Li^+ solvation behaviour will affect the formation of electrolyte interface together.[9,72] Initial specific adsorption existing on the surface of the electrode will determine the initial chemical composition and structure of the EEI, while the solvation structure of Li^+ is involved in the dynamic evolution of the EEI, and the interaction between them affects the stability of the EEL together.[73,74]

It is generally accepted that the metal or oxide trend to lose electrons until the dynamic equilibrium is reached if the electrode once contacts with the electrode. The interfacial area of the electrode and the solution where excess charge accumulates is defined as the EDL.[75,76] The concept of EDL was proposed and modelled by von Helmholtz in 1853, and was modified by Gouy, Chapman, and Stern.[75,76] Stern divides the EDL into compact layer and diffusion layer. The compact layer includes inner Helmholtz Plane (IHP) and outer Helmholtz Plane (OHP).[77] The specific adsorption of solvent molecules and anions exists in the IHP in the initial state of the electrode. It's also limited by the limited space in the IHP, which can't contain solvation groups. There is no specific adsorption phenomenon in the OHP, but there are groups with solvation structure. The Helmholtz plane is the closest position to the electrode for the reaction substrate such as the specific adsorption ions and solvated structure, and it is also the main place for the oxidation/reduction reaction of ions and electrons in the initial solution. There is no denying that most cations (Li^+, K^+, Na^+, Al^{3+}, etc.) own the strong ability to coordinate with solvent molecules to form solvation groups, compared to anions which are difficult to be solvated due to the poor matching with solvent molecules. Therefore, it can be concluded that anions are more favourable to be adsorbed on the electrode surface without combining with solvents. In the current study, it is meaningful to explore the deep understanding about the featured specific adsorption on the inner Helmholtz plane of electrode surface, since they play significant roles in forming a stable interface.

Yan et al.[9,72] reported that the property of the specific adsorption in EDL may exist only in the battery for the first cycle, and then it will be replaced by the electronic insulated EEI, as an important bridge between electrode and electrolytic liquid phase. The initial state of IHP ion specific adsorption of the electrode will directly related to redox reaction of electrode/electrolyte interface so that affects EEI structure and chemical composition.

In addition to the specific adsorption, the solvated structure of Li^+ is another important factor of the EEI.[78–80] For the EEI forming process, the electrolytic liquid phase of the solvation structure has significant effects in the formation of EEI. Recent evidence suggests that Li^+ tends to form solvation structure with strongly polar solvent molecules in low concentration electrolyte, while anions are excluded from the solvation sheath. However, in high concentration electrolyte, the anions are more likely to enter the solvation sheath. Compared with chain solvent molecules and anions, cyclic solvent molecules are more likely to form solvation structures when they coordinate with cations (Li^+, K^+, Na^+, Al^{3+}, etc.) in dilute solution. And these electrolyte components involved in the solvation structure, especially those entering the inner solvation layer, will participate in the formation of EEI, thus affecting the structure, composition, ionic conductivity and thickness of the EEI.[44,78,80–86] Yao et al.[87] successfully prepared a weakly solvating electrolyte (WSE), which realized the formation of a large number of ion pairs and polymers in the electrolyte at low salt concentration, and allowed more anions to participate in the solvation sheath at low salt concentration. A unique anion derived electrode interface is formed on the graphite electrode, which can realize the performance of fast charging and long-term stable cycle. By using first-principles calculations, they reveal the competitive coordination of anions and solvent molecules to Li^+ in the solvation structure, which provides a new insight for the development and design of new electrolytes in the future.

Li^+ intercalation into graphite

During the charging process, Li^+ will remove from the cathode and then intercalate into the graphite anode through the electrolyte. However, SEI will be formed on the graphite electrode before the Li^+ intercalate into graphite as mentioned above, which will have a great influence on the insertion and plating of Li.

It is well acknowledged that the charging process of graphite anodes can be divided into 4 sequential steps at an atomic scale (Figure 4a).[48,88]

(1) The solvated Li^+ moves in the bulk electrolyte, especially through tortuous channels and micro pores in graphite

DOI: 10.54227/elab.20220011

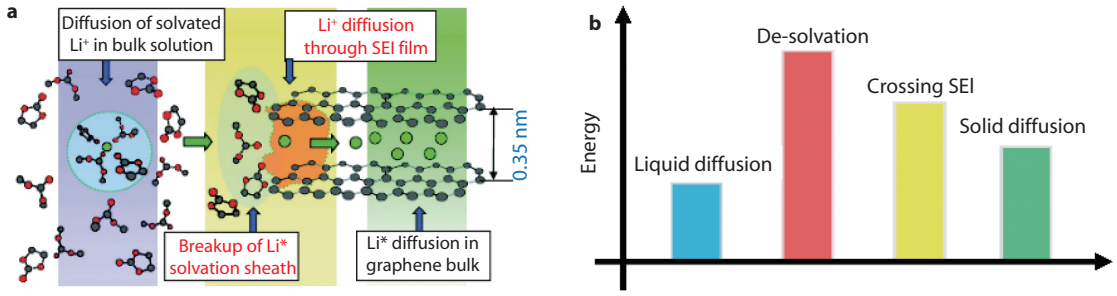

Fig. 4 **a** Schematic diagram of Li-ion intercalated into graphite during charging.[48] Copyright 2010, American Chemical Society. **b** Energy diagram corresponding to the 4 sequential steps of **a**.

electrodes.

(2) Once the solvated Li^+ reaches the interface of graphite/electrolyte, charge transfer cannot immediately proceed due to the existence of an electron-insulating SEI. The solvation sheath of Li^+ must be stripped off before crossing the SEI, which is termed as the de-solvation process.

(3) Naked Li^+ diffuses through the mazy SEI and intercalates into the layer of graphite.

(4) The diffusion of Li^+ within graphite galleries, accompanied by electron transfer and rearrangement of the graphite lattice (from AB stacking to AA stacking).

According to the 4 steps mentioned above, the limiting factors of faster insertion Li^+ into graphite can be generally categorized into the following two types:

(a) Mass transport: This mainly includes the diffusion of Li^+ in both electrolytes and carbon materials, which is (1) and (4) in this case.

(b) Charge transfer: The transport of Li^+ across SEI can form a major kinetic barrier, which consists of (2) and (3) for graphite anodes. For this reason, it is essential to decouple the influence of mass transport and charge transfer to identify the rate-determining step.

Concerning the energy barrier of the two limiting factors (Figure 4b), the solid diffusion of Li^+ in graphite lattice is limited by energy barriers in the range of 20–40 kJ mol^{-1}, which is reported to increase with the degree of lithiation.[26] However, the energy of de-solvation in various cathode materials and graphite is similar (50–70 kJ mol^{-1}) when the carbonate electrolytes are used.[89–91] But the de-solvation energy barrier can be changed with the temperature and composition of electrolyte. So far, however, there has been little discussion about the energy barrier for Li^+ to cross the SEI, because the properties of the SEI drastically change with the composition of electrolytes, especially for the solvents, lithium salts and electrolyte additives. For example, it was once reported that the energy barrier for Li^+ to cross the SEI is about 20 kJ mol^{-1}, but no more solid and subsequent researches have confirmed that.[88]

To date there has been slight agreement on whether mass transport or charge transfer is the major limiting factor during charging process. Firstly, there are many variables (such as charging rate, working temperature, electrode material and thickness, and so on) in the battery test, which can be changed the dominated factor. To be specific, mass transport play a leading role in the overall intercalation kinetics for thicker electrodes or at larger current densities[92,93], whereas charge transfer could possibly become the limiting factor when charging thin electrodes especially at sub-zero temperatures because of the increasing activation energy.[47,49] Therefore, the battery test conditions need to be emphasized when differentiating the rate limiting steps. Secondly, the de-solvation process cannot be recognized as the rate determining step, while it is the step that need the most activation energy. This is because the rate constant is not only a function of activation energy, but also the pre-exponential factor, according to the Arrhenius equation.[94] That is to say, the rate constant is another index to determine the chemical reaction rate, except for the energy barrier.

On the basis of these results, what we can summarized as follows: (1) The process of Li^+ intercalation into graphite is related to various cell parameters (electrode thickness, electrode material, temperature, areal loading, and so on). The test condition must be given before declaring the rate determining step. (2) The rate determining step will not exist and the charging process can be controlled simultaneously by more steps if both processes contribute similarly. (3) It should pay more attention to further mechanistic studies and the experimental equipment for exploring the rate determining step. And it will supply more solid conclusion to find the key factor of rate determining step theoretically or experimentally.

What do we know about Li plating?

Cognitive process of Li intercalation and plating in past 50 years

Our current analysis and prediction of the phenomenon of Li plating on graphite electrode in LIBs are accompanied by an understanding of graphite intercalation chemistry. The rough cognitive process is revealed in Figure 5. The whole stage can be divided into 4 parts. The first part was that people began to realize that Li^+ would magically insert in graphite layers and form GICs. This is a fundamental finding, but it will be a cornerstone of subsequent research. In 1970, when Dey et al.[95] verified the decomposition products of propylene carbonate (PC), they found that when a large current passed through the circuit, in addition to intercalation of Li^+ in graphite, atomic Li deposition also occurs on the graphite surface. In a sense, it is the first time for LIBs to monitor the Li deposition behaviour on the graphite electrode under high applied current. Hu et al.[39] reported that Li atoms can diffuse into bulk graphite and form a Li-graphite sub-monolayer

DOI: 10.54227/elab.20220011

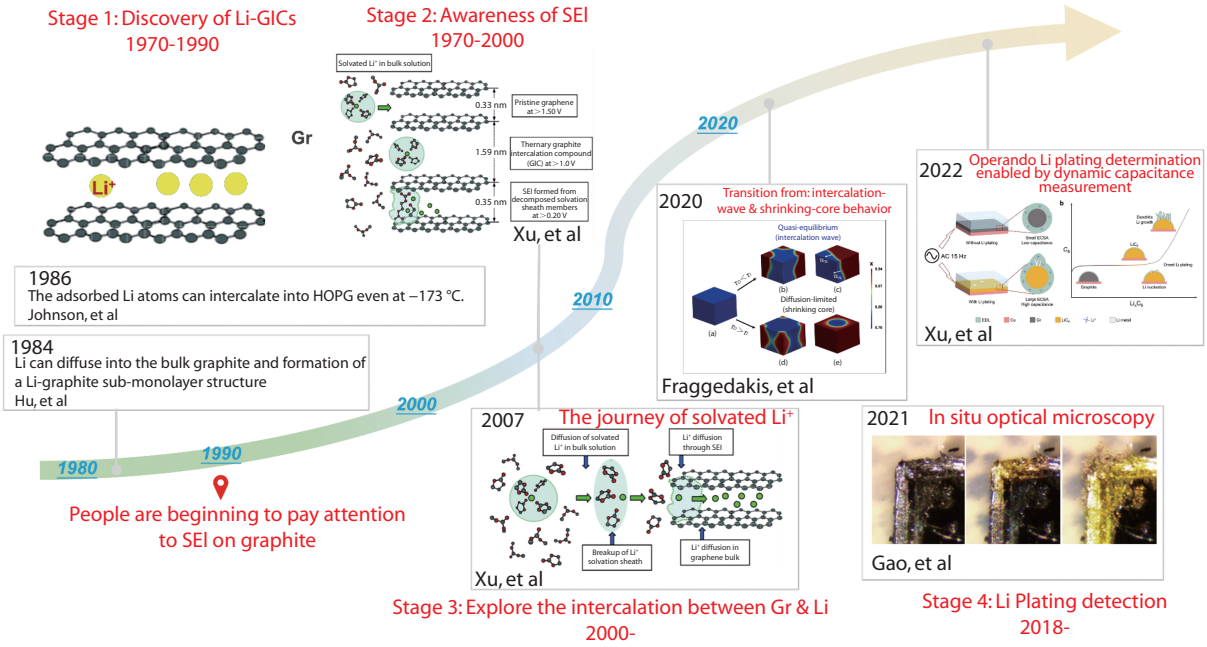

Fig. 5 Cognitive process of Li intercalation kinetics and Li plating in past 50 years. The copyright claims for the images are listed in the order of the year mentioned. Copyright 2007, American Chemical Society.[88] Copyright 2020, Royal Society of Chemistry.[43] Copyright 2021, Elsevier.[51] Copyright 2022, John Wiley and Sons.[104]

structure, thereby changing the electronic configuration from metallic Li to a configuration similar to that of Li compounds in 1984. It showed that Li can be combined with graphite to form a compound. Two years later, Johnson et al.[40] evaporated Li metal onto HOPG and found that Li atoms can transfer part of the outer layer charge to graphite, and Li forms an intercalation compound in graphite. At the same time, the behaviour of Li intercalation into graphite can occur even at −173 °C. Then people began to realize that there seemed to be something at the graphite/electrolyte interface. This substance determines whether graphite can maintain a stable structure under different electrolyte conditions. As discussed earlier in this article, this substance was identified as SEI and has been extensively studied from ~1970 to 2000. In 1999, Arora et al.[96] pointed out that when the potential of the graphite electrode reaches below 0 V, it is thermodynamically feasible for Li to be deposited on the graphite surface. In the next year, Huang et al.[97] proposed that the slower diffusion process of Li^+ in carbon anode materials is the reason for the poor performance of LIBs at low temperatures, rather than the limitation of the mass transfer process in the electrolyte or passivation film.

In the 21st century, due to advances in characterization and calculation methods, research on LIBs has become more in-depth. Since 2000, many researchers have systematically studied the interaction between Li^+ and graphite from interface and graphite electrode. In 2005, the authors predicted that the Li flux of the charge transfer reaction at the SEI would be higher than the Li diffusion flux intercalation into the bulk graphite, which would then cause Li^+ to accumulate at the interface between the graphite electrode and electrolyte and the metallic Li deposition.[98] In 2006, Zhang et. al.[99] experimentally proved that Li deposition will occur under most charging conditions, especially under high-rate and low-temperature. From this work, the term for Li deposition on the graphite surface changed from Li deposition to Li plating. Xu[47] proposed the journey of solvated Li^+ from solution to graphite, and the impedance components related to each step in 2007. In 2010, Xu et al.[48] mentioned that the desolvation process was the main energy-consuming step during Li^+ transport process. In 2012, some researchers pointed out that the energy barrier of the Li sub-monoatomic layer on the graphite surface diffused into the graphite layer was very low (only 0.16 ± 0.02 eV).[42] Two years later, Legrand et al.[100] studied the Li plating behaviour that cause aging and life decay of LIBs, and attributed the cause of Li plating to the charge transfer process and the solid phase diffusion of Li^+. The solid phase diffusion of Li^+ between the graphite layers occurs on a longer time scale, compared to that of the charge transfer process. It was believed that charge transfer is the rate limiting step of the insertion of Li^+ in the negative electrode active material, resulting in subsequent Li metal deposition on graphite particles. With the increase of the harsh working conditions of LIBs, people begin to pay attention to the problem of Li plating on graphite anode. Since 2018, more work has been focused on the detection and mechanism analysis of Li plating. In 2019, Duan et al.[101] conducted research on whether graphite is lithophilic or lithiophobic. The authors proposed that HOPG itself is lithophilic and Li can be intercalated into the graphite layer through the grain boundary or plane defects of graphite. Therefore, the intercalation of Li in HOPG is a spontaneous process, which also helps the spread of liquid Li metal on HOPG. At the same time, authors study the wettability of molten Li droplets on pre-lithiated porous graphite paper (PCP) and graphite powder through design experiments. It was proved that when the phase structure of graphite changes (from C_6 to LiC_6), the lithiated material has super-lithophilic characteristics.

DOI: 10.54227/elab.20220011

By 2020, a special year, the work of many researchers has given us a deeper understanding of Li plating. In this year, Liu et al.[102] studied the influence of current density on the local Li plating behaviour by designing separators with different diffusion gaps in coin cells. It was found that as the current density increased, the critical size for uneven electroplating was gradually reduced. Besides, it was reported that the migration of Li^+ has a great influence on the accumulation of Li at the graphite anode. Subsequently, Wang et al.[103] used a special coin cell configuration with adding hot spots to explore the influence of the temperature unevenness on Li plating. The study found that the deposition of Li metal is prone to occur in local high temperature areas caused by hot spots, which may be caused by the coupling of thermodynamic and kinetic effects. On the one hand, because the thermodynamic equilibrium potential is closely related to temperature, local high temperature causes the increment of the equilibrium potential Li/Li^+, which also lifts the thermodynamic onset for the deposition of metallic Li. On the other hand, due to the faster Li^+ movement rate and large exchange current density at the hot spots, it further promotes the occurrence of Li intercalation into graphite and Li plating. Besides, Fraggedakis et al.[43] introduced two ways of phase transition in ion intercalated materials from intercalation-wave (quasi-equilibrium) to shrinking-core (diffusion-dominated). It was also proposed that the process of graphite inserted with Li^+ is carried out in the form of the latter. After that, Gao et al.[51] used *in-situ* optics and phase field simulations to study the lithiation process and the behaviour of Li plating utilizing a single graphite particle. They believed that the Li plating was caused by the saturation of Li intercalation on the surface of the graphite particle. That is to say, solid diffusion plays an important role in Li plating. When it comes to the boundary of safe Li plating in LIBs, Cai et al.[25] proposed that the capacity of Li plating should be controlled <25% graphite capacity, under the condition of ~95% coulomb efficiency of Li metal deposition/dissolution. The metallic Li deposition on graphite electrode is considered to be a key bottleneck for faster charging which is a key enabler of economic success of EVs. Recently, considerable research efforts have been devoted to the investigation of onset/detection of Li plating, mechanism of Li deposition and so on. For instance, a pathbreaking technique, dynamic capacitance measurement, was proposed by Xu et, al. for detecting the deposited Li metal at 2022.[104]

Factors affecting Li plating

It is well acknowledged that the operating potential of the graphite anode (~0.1 V vs. Li/Li^+) is above 0 V in terms of thermodynamics. However, the potential of graphite electrode will drop down to less than 0 V due to abundant polarization under the condition of low temperature, high charging rate and high state-of-charge (SOC), leading to the deposition of Li metal on the graphite particles.

The related Li intercalation and Li plating reactions are presented as bellow.

$$\delta Li^+ + \delta e^- + Li_xC_6 \rightarrow Li_{x+\delta}C_6$$

If $x+\delta < 1$, it means that there is enough space between the graphite layers for Li^+ to occupy so that the Li^+ can be normally intercalated into the graphite. If $x+\delta > 1$, it means that the number of Li^+ exceeds the number of graphite available places, the excess Li^+ will not be inserted into the graphite, and thus converted to Li metal, which is deposited on the graphite. Arora et al.[96] first proposed a Li deposition model for Li_2MnO_4/C LIBs based on Newman's theory, which divided the current density of the anode into two parts: Li intercalation current and Li plating current.

At present, there are 4 mechanisms of Li plating on graphite electrode (It must be pointed out that due to the interaction between dynamics and thermodynamics, the above 4 mechanisms are coupled rather than independent.):

(1) The Li plating reaction will be thermodynamically possible when the potential of graphite drops down to 0 V (vs. Li/Li^+) due to the difficult intercalation process which results large overpotential exceeding the equilibrium voltage of the Li-graphite phase in stage1.[96]

(2) Li plating could be caused if local salt depletion near graphite surface, which triggered large concentration polarization leading the voltage of graphite below 0 V, and the depletion of Li^+ is favourable for dendritic Li deposition.[105]

(3) Li plating could occur when intercalated Li^+ saturate the graphite surface and block further insertion due to the slow solid diffusion compared to insertion.[51,100]

(4) Li plating could be affected by charge-transfer process included the de-solvation process and Li^+ crossing the SEI. And it is in favour of Li deposition under high charge transfer resistance.[48,106,107]

In addition to the 4 common factors mentioned above, other precipitating factors such as dissolution of transitionmetal ion (especially manganese ion) from cathode will also lead to Li plating on graphite anode.[108] The mechanism of Li plating on graphite electrode is straightforward to understand, but the cause of Li plating under different working conditions (high SOC, high charging rate, and low temperature) has not been explained uniformly.

High state of charge

It is found that the mass of plated Li was linearly dependent for the SOC values by analysing the differential voltage analysis of discharging voltage profiles after charging.[109] It was also noted that reversible plated Li was less when charging to relatively high SOC. To gain more insight, linear regression was applied for the determination of growth rate and initiation point of Li plating, and decreasing temperature led to higher growth rates and shifted the initiation point to lower SOC which meant that the plating process starts earlier.

As can be seen from Figure 6, a simplified model of the Li plating-stripping process at different SOC levels is given. The regionally plated Li keeps good electrical contact with the bulk of graphite electrode at low SOC, so that most of the metallic Li can be re-intercalated into the graphite with less irreversible Li. However, the plated Li can grow through the SEI and get in contact with the electrolyte given sufficient time at medium SOC, which will cause capacity losses due to the new surface film formed and isolation of dead Li during discharge. The intercalation reaction exceeds Li plating due to low charge currents at high SOC, which leads to a porous structure of deposited Li near the electrode surface. These structures provide finite electrical contact. The porous Li deposits close to the electrode surface are oxidized firstly during discharge. More distant Li structures are thus easily isolated from

DOI: 10.54227/elab.20220011

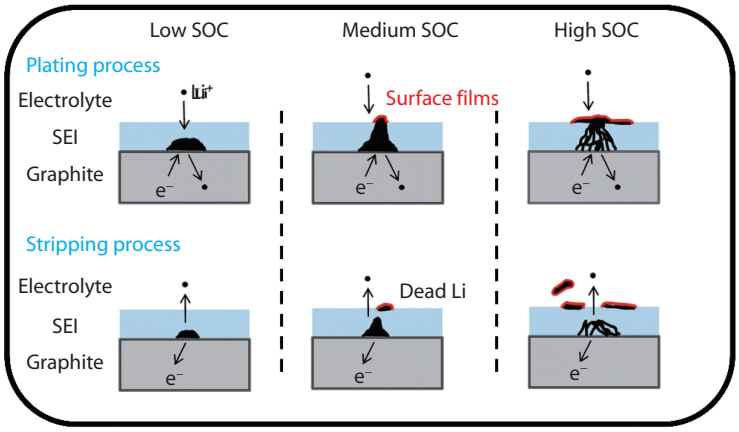

Fig. 6 Simplified model of the lithium plating-stripping process at different SOC levels.[109] Copyright 2014, Elsevier.

the graphite electrode and result in dead Li.

Furthermore, Persson et al. found that the diffusion barrier is increased by x in Li_xC_6[46], which will constraint the intercalation kinetics under higher SOC. As will be described below, the slow solid diffusion of Li in graphite plays an important role in Li plating.

To gain more insight, the intercalation process of Li in a single graphite crystal was observed by *in-situ* optical observation.[51] It is found that no deposition of Li occurs when the surface potential of the graphite particles reaches below 0 V (vs. Li/Li$^+$). However, when the outer regions of the graphite particles become golden yellow for a period of time, that is, when the edge plane of the graphite reaches saturation, Li plating will occur. The author also deduced the potential of graphite electrode under certain conditions by utilizing the chemical potential:

$$V \approx -\frac{\mu_s}{e} + \eta_w$$

Here, V is the potential of graphite electrode, μ_s is the chemical potential of inserted Li at the graphite surface. To drive the reaction, a negative overpotential η_w occurs to lift the energy of Li$^+$. The voltage derived of graphite electrode reflects the thermodynamics and kinetics of Li intercalation and deposition process. And authors divided the lithiation of graphite into four parts: open circuit, Li intercalation, Li nucleation, and Li growth (Figure 7a):

(a) Open circuit: The chemical potential of intercalated Li,μ_s, is much lower than the chemical potential of metallic Li, μ_{Li}, without applying current.

(b) Li intercalation: As more Li$^+$ intercalate into the graphite, there are existing sequential phase transformation at the surface of graphite due to the incremental surface concentration, so that the graphite surface will become more crowded, with μ_s and the magnitude of the over-potential increasing accordingly. As a result, the energy of the reactants increases, and the potential decreases.

(c) Li nucleation: Li intercalation becomes kinetically difficult because there is no more available site in graphite for Li$^+$ to occupy, which is favourable for the nucleation of metallic Li. And the potential of graphite drops down to its minimum.

(d) Li growth: Li metal begins to grow based on the Li nuclei due to the much smaller activation energy than nucleation, so that the reduction reaction is mainly caused by the growth of Li metal. The potential of graphite electrode is lower than 0 V (vs. Li/Li$^+$) with the required overpotential for the growth of Li metal.

Based on the derivation of the potential of graphite electrode above, it can be deduced that the diffusion chemical potential of the corresponding Li$^+$ in the graphite is 0 V (vs. Li/Li$^+$) when the graphite edge plane is saturated with Li. Under the drive of overpotential, the potential of the graphite electrode at this time must be below 0 V (vs. Li/Li$^+$) since the overpotential driving Li$^+$ intercalation itself is negative. In this case, Li plating will definitely occur. However, the Li deposition occurring is thermodynamically possible when the potential of graphite electrode reaches below 0 V, it does not necessarily mean the deposition of Li metal. Therefore, it can be seen that solid diffusion is another key factor to induce Li plating.

High charging rate

In order to achieve fast charging, high-rate charging will trigger a series of side reactions, such as Li plating, mechanical effects, and heat generation, which are the culprits that cause uncontrollable problems in the battery and accelerate aging.[25,110–112] This is demonstrated in numerous studies that the high charging rate facilitates Li plating. Note that Konz et al.[113] recently studied the effect of different charge rates of 2 C, 3 C and 4 C on the Li plating occurrence of LIBs with graphite, which revealed Li plating could be observed at the beginning of 75%, 50% and 25% SOC during charging process for 2 C, 3 C and 4 C charging rate, respectively (Figure 7b).

And a number of researchers have reported that the lithiation process is largely depends on the solid diffusion of Li$^+$ in graphite under the increasing charging rate. That is to say, the charging rate is mainly limited by the Li$^+$ intercalation kinetics at the graphite anode during fast charging.[85,98,102] The high current density can trigger a large activity gradients of Li$^+$, while the depletion of Li$^+$ who intercalates into graphite is relatively small.[114,115] Thus, a large number of Li$^+$ will accumulate on the electrode/electrolyte interface due to the lower Li solid diffusion coefficient compared to the Li$^+$ diffusion coefficient in electrolyte. Inserted Li$^+$ can hinder latter Li$^+$ intercalation when the intercalated Li accumulates at the border of graphite.[115] Further, the accumulation of Li$^+$ triggers a large concentration gradient at the interface of graphite so

DOI: 10.54227/elab.20220011

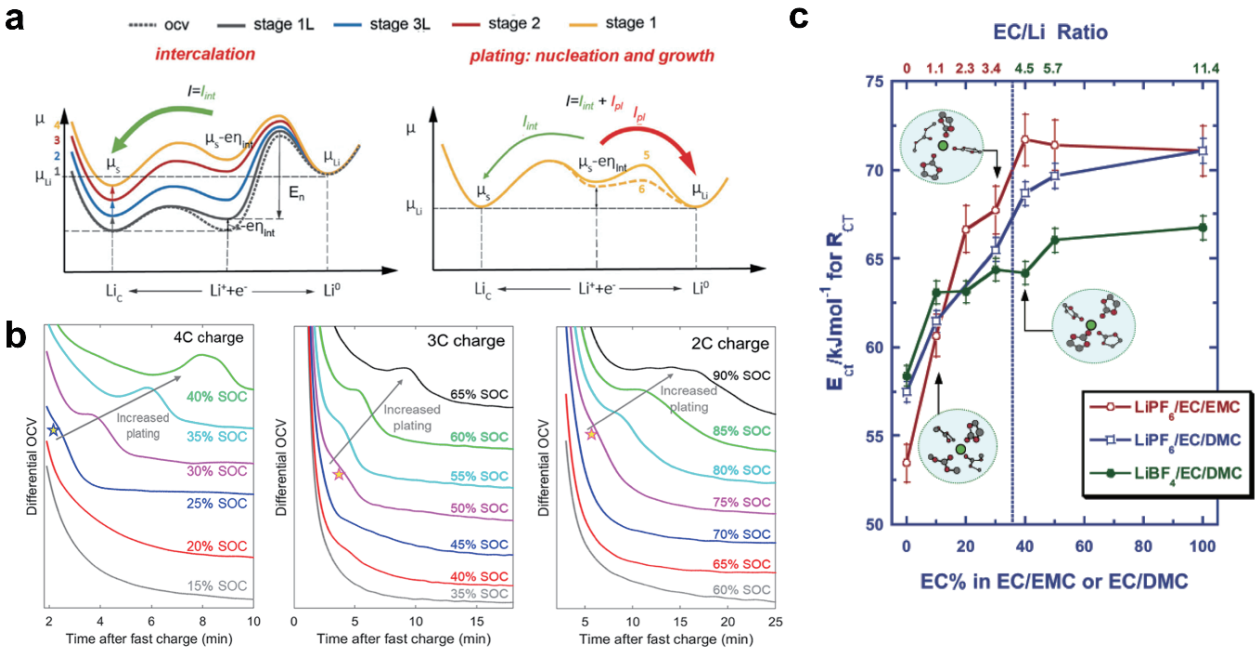

Fig. 7 **a** Reaction energy landscape before plating occurs (left) and after plating starts (right).[51] Copyright 2021, Elsevier. **b** Detecting the onset of Li plating at 4C, 3C, and 2C in graphite/Li cells by using differential OCVs.[113] Copyright 2020, American Chemical Society. **c** Relationship between the activation energies associated with so-called charge-transfer process and the EC/Li molar ratio: the relationship between Li^+ solvation sheath composition and the EC content in the solution.[88] Copyright 2007, American Chemical Society.

that Li deposition occurs more easily if the surface of graphite is saturated of Li^+.

However, debate continues about the rate limiting factor during high charging rate. Some reports point that the charge transfer kinetics would dominates the high charging rate process, rather than the Li diffusion in carbon materials.[100,116] As mentioned in chapter Li^+ intercalation into graphite, the rate determining step of fast charging can be varied with cell parameters (electrode material, electrode thickness, areal loading, temperature, and so on). It is still a controversial topic to distinguish the solid diffusion and charge transfer process.

Low temperature

There is no denying that the performance of LIBs will be poor at low temperature, due to the increased charge transfer resistance, high resistance SEI film and slow Li^+ diffusion.[107,117–124] The mentioned conditions are favourable for Li plating. Despite the behaviour of LIBs at low temperature have been systematically studied, the inducing factor of Li plating on graphite anode is poorly understood.

According to the Arrhenius law, the probability to overcome the barrier gets lower with decreasing temperature so that Li deposition on the graphite anode is much easier appeared compared with intercalation under low temperatures.[29,31,115,120,125] Previous study has reported that a coin cell model was charged at −25 °C (from 0% to 60% SOC and 80% SOC respectively) and −20 °C (from 0% to 80% SOC) under 1.5 C-rate, which found the lithium plating ratios, defined as the ratio between the charge corresponding to Li plating and the total charge, were 1.15%, 1.55% and 0.92% respectively.[106] The model indicated that Li plating occurs even at SOC lower than 10%, before the Li^+ concentration at the surface of graphite particles becomes saturated. Notably, it is also mentioned that the reason why Li deposition more easily appears when charging at low temperature could be further attributed to the decreased exchange current density of insertion reaction, which causes the difference of solid phase potential and electrolyte phase potential smaller than the thermodynamic equilibrium potential of Li/Li^+ (0 V), leading to the Li plating.

It is also important to highlight that most studies in the field of graphite-based LIBs are based on the ethylene carbonate (EC) mixtures due to its distinguished ability to stable the graphite/electrolyte interface, which is needed for good performance LIBs.[126,127] Besides, in high charging rate and low temperature condition, it is reported that EC can be added to well passivated the plated metallic Li so that there was no gas resolution in EC-based electrolyte compared to the sharply increased volume of pouch cells in EC-free electrolyte.[128] Until now, there is no denying that the most widely utilized electrolyte in LIBs are based on $LiPF_6$ and mixtures of cyclic carbonate (EC dominated) and linear carbonate solvents, such as dimethyl carbonate (DMC), diethyl carbonate (DEC), or ethyl methyl carbonate (EMC) at all, which ensure the electrolyte have lower viscosity and the higher ionic conductivity. Although EC is widely used in electrolytes of LIBs, it has many limitations, such as high viscosity and melting point, which will result in poor performance LIBs at low temperatures. Further, due to EC is indispensable in electrolyte, the graphite/electrolyte interface will be importantly

DOI: 10.54227/elab.20220011

affected, and this influence will bring difficulties to distinguish the real factor caused Li deposition at low temperature.[88] And Xu investigated the effect of the solvent ratio (ratio of EC to DMC) on the activation energy of charge transfer process in order to supply a guideline to develop state-of-the-art electrolyte of LIBs using in low temperature.[47] The structure of cyclic carbonate (EC) interacts stronger with Li^+ compared to the linear carbonate (DMC) so that the charge transfer activation energy of $LiPF_6$/EC and $LiBF_4$/EC solutions are 65–70 kJ mol^{-1} and <60 kJ mol^{-1} respectively. As displayed in Figure 7c, there is an interesting discovery that the Li^+ solvation sheath would be dominated by EC if the ratio of EC exceeded 30%, while the liner carbonate DMC would participate in the solvation process when the EC content decreased to >30%. It was proposed that the activation energy of the charge transfer process shifted from ~70 kJ mol^{-1} (with $LiPF_6$) and ~60 kJ mol^{-1} (with $LiBF_4$) to less than 60 kJ mol^{-1} where EC content at 20%–40%.[48,129] Furthermore, the deposition composition on Ni electrode was exclusively made up by the reduction product of EC with EC/EMC=30:70.[130] And the SEI components could come from the reduction of DMC only in the system of $LiBF_4$/DMC or $LiPF_6$/DMC electrolytes.[131]

From the above discussion, we can determine that EC is a good SEI-forming solvent for graphite electrodes, and its addition will have a significant impact on the graphite/electrolyte interface. Up to date, EC cannot be easily removed from the commonly used electrolyte system. However, the existence of EC will slow down the migration rate of Li^+ at low temperatures and increase the activation energy barrier of de-solvation (increase the charge transfer impedance). These factors will lead to Li plating in LIBs at low temperatures. Therefore, the search for an electrolyte system without EC, and with good SEI formation and passivation characteristics of metallic Li will bring a new breakthrough in the research of low temperature LIBs.

On the other hand, mass transfer process, especially the Li^+ solid diffusion in graphite, also limits the performance of LIBs at low temperature[118]. The diffusion coefficient (D_{Li+}) in a graphite electrode could be reduced to only 12% of that at room temperature during the cycle at −20 °C.[124] Besides, the D_{Li+} in graphite at −32 °C was reported to 10^{-13} cm^2 s^{-1}, compared to the 10^{-8} cm^2 s^{-1}at room temperature determined by intermittent titration technique (GITT)[132]. By the way, most of the paraments are measured under the equilibrium states due to practical constraints, so that these testing values cannot reflect precisely the real kinetic process of LIBs at low temperature.

When it comes to the commercial batteries, it is exhibited that Li plating starts at a 2 C charging rate for 50 °C, compared with 0.5 C-rate at 12 °C.[133] It is worthwhile mentioning that low temperatures are also likely to slow down the reaction of plated Li with electrolyte as well as chemical intercalation of Li into graphite. It is also interesting to note that the plated Li can be re-intercalated into graphite during relaxation, but the process can be restricted especially at low temperatures which slows down the relaxation. The reversibility of metallic Li is so fine that the process of re-insertion cannot be observed at higher temperature (>25 °C).[29]

Nevertheless, for the adverse effect of LIBs induced by low temperature as mentioned above, the behaviour of LIBs under high temperature cannot be overlooked. To date there has been little agreement on whether Li plating occurs at high temperatures. Some researchers showed that local plating could be observed at high temperatures (>45 °C)[29,134–136], while others held the view that the metallic Li deposition can be avoided at high temperature.[137]

It should be noted that the uneven temperature on electrode can make local Li plating thermodynamically favourable even at room temperature due to the contribution of thermodynamics and kinetic. This research links the uncertainty of Li plating to thermodynamic factors Surveys such as thermal gradient induced Li plating that conducted by Fear et al.[138] presented that in-plane thermal gradients strongly influence active material utilization, while the inter-electrode thermal gradients could result in a shifting on the solid phase potential at each electrode during charging. Besides, they found Li plating can be exacerbated if the cathode temperature exceeds the anode temperature, which could accelerate battery degradation. And Angeles et al.[117] used a 3D microscopic electrochemical model to predict the Li plating onset at low temperature, and pointed that Li plating could occur in larger cells and cylindrical cells due to heterogeneous potential distribution.

Other factors

The design of battery configuration and electrolyte composition will affect the deposition of Li metal. In pouch cells, higher current density near the current collector tab is favorable for local Li deposition. And the locally plated Li near tab can increase the thickness of pouch cell due to the incremental Li deposition.[139]

From the electrode scale, many works reported that metallic Li is more likely to deposit on the edge of the graphite anode, while the center area of the graphite anode remains unused. Tang et. al. pointed that this phenomenon is caused by the geometric effects. In commercial LIBs, the size of graphite anode is generally larger than that of cathode, causing a larger current density and a large over-potential at the edge of the graphite electrode so that marginal Li deposition is favorable.[140] However, another explanation for the marginal deposition of Li based on smaller graphite anode compared to cathode. It is reported that graphite anode was overcharged due to an uneven concentration distribution at the overhang area between anode and cathode. These findings are mainly based on a major premise that the electrolyte distribution on the graphite electrode is uniform. And Yang et al. investigated the overlooked effect of nonuniform distribution of electrolyte on Li plating during fast charging.[141] It was found that metallic Li is prior plating on the saturated Li-graphite compounds in the anode region with sufficient electrolyte since the Li^+ transport is blocked in the anode region lacking electrolyte.

In addition to above factors, defects introduced in production process, like uneven thickness of electrode and impurities produced during packaging, are the potential pitfalls for local Li plating. According to the research of Cannarella et. al., it was reported that the separator pore closure could cause local Li deposition. Based on their study, the authors showed the pore closure acts as an electrochemical concentrator which can induce high current and overpotential, so that the

DOI: 10.54227/elab.20220011

Li plating is favorable.[142] Of course, there are many other factors that can induce Li deposition. In order to avoid the influence of plated Li on battery safety, it will bring strict requirements for electrode preparation and battery assembly.

What is the adverse effect induced by Li plating?

After Li deposition on the graphite electrode, there are 2 major hazard effects on LIBs:

(1) Thicker SEI: Metallic Li will react with electrolyte to form SEI, which blocks the pores of ion transport among graphite particles due to the thicker SEI on the surface of plated Li and limits the intercalation kinetics. Thus, a positive feedback mechanism is generated so that Li plating more easily occurs on graphite electrode.

(2) Dead Li: Electrically disconnected Li (dead Li) can be generated during the process of plated Li re-inserted into graphite and Li stripping. And the thicker SEI on Li metal surface is in favour of the formation dead Li as well, because SEI blocks the path of Li from gaining electrons.[143]

The hazards of the 2 effects mentioned above will seriously threaten the performance of LIBs, leading to battery aging and even safety problems. For the LIBs performance degradation caused by Li plating, the inducement can be analysed from the following aspects (see Figure 8a). First of all, when the metal Li is deposited on the surface of graphite, the available active Li in the LIBs will decrease. At the same time, the electroplated Li metal will generate more SEI and dead Li, which will lead to the blockage of the channel transporting Li^+ among the graphite particles. Besides, the internal resistance (R) of the battery will increase, and the capacity (Q) and Coulombic efficiency (CE) of the battery will be reduced. In addition, although the plated Li metal can be inserted back into the graphite to restore a part of the battery capacity, the vast majority of electroplated Li will become inactive Li under the condition of high charging rate, low temperature and high SOC, which is unable to re-intercalate into graphite.

When it comes to the safety issues caused by Li plating, thermal runaway (TR) and even exploding of LIBs are a major concern in public. It is generally accepted that thermal runaway of LIBs is triggered by a series of chain reactions of materials within a battery, whose temperature contributes mainly by internal short and the reaction between electrolyte and electrodes.[144–149]

The TR caused by Li deposition side reaction is depicted in Figure 8b. In the process of thermal runaway, the 3 stages for the continuous temperature increment of the LIBs are as follows[19]:

(a) Stage 1 (60 °C–110 °C): The metallic Li react with electrolyte which is an exothermic process, and the SEI on plated Li undergoes constantly breaking up and regenerating, while the temperature in LIBs during this stage rise slowly.

(b) Stage 2 (110 °C– ~200 °C): The reaction between plated Li and electrolyte becomes consuming so that the heat release sharply at the same time. The amount of heat generated at this stage will cause the separator melting, bringing the anode and cathode into direct contact. Further, the heat generated at this stage will push the battery to the critical TR temperature.

(c) Stage 3 (>200 °C): If the battery continues to produce heat, it will reach an irretrievable thermal runaway temperature, at which point the material within the battery will react with each other. There are violent reactions between the anode and the electrolyte, the cathode and the electrolyte, and the anode and the cathode. Eventually, the battery will reach the highest temperature of TR, and the battery will catch fire or even explode.

According to the above conditions causing TR of LIBs, the Li plating on graphite anode cannot be ignored, because it can accelerate the rate of TR. When overcharging or applying higher current density further aggravates the side reaction of metal Li deposition and increases the temperature of the battery sharply. Besides, when the temperature in battery continues to rise, the gas generated by the decomposition of the electrolyte causes the internal pressure of LIBs to rise continuously. Eventually, high temperature causes the battery to deflate and the Li metal to melt. In this process, water and oxygen in the air react violently with the metal Li, leading to combustion and even explosion.[29]

How to monitor Li plating?

Because of the harmful effects of Li deposition on LIBs, it is very important to monitor the occurrence of Li plating. At present, the detection methods of Li plating in LIBs can be generally divided into two categories. One is the *in-situ* or *operando* monitoring methods of battery charging and dischar-

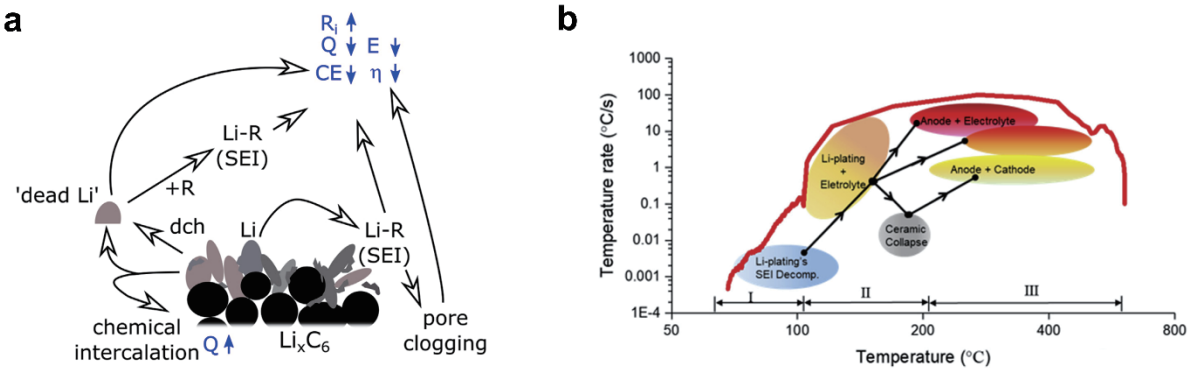

Fig. 8 **a** Ageing mechanisms related to Li deposition in Li-ion cells.[29] Copyright 2018, Elsevier. **b** Chain reactions of the thermal runaway process in fast charged LIBs.[19] Copyright 2019, Elsevier.

DOI: 10.54227/elab.20220011

ging process utilizing different experimental methods to identify the occurrence of Li plating. These *in-situ* detection methods have strong persuasiveness because it can reflect the actual working state of the battery and can monitor the behaviour of Li deposition in real time. The other means of detection is generally divided into *ex-situ* test methods. Generally, the battery should be disassembled and characterized by different instrument after the cycling. Although the *ex-situ* method can capture the situation of Li plating more directly, it cannot reflect the onset of Li plating in real time of LIBs.

in-situ detection method

For the electrochemical/chemical behaviour of Li (re)intercalation, deintercalation, and deposition, there are signals associated with more readily available voltage/current curves (along with information such as impedance or capacity of LIBs). Compared with X-ray and other methods, it is simpler and more accurate to analyse the electrochemical information data by various methods. At the same time, the information of the battery under different working conditions can be obtained in real time.

The Li deposition on graphite electrode rather than intercalation into graphite will consume a large number of active Li^+ so that the CE has a sharp drop. The high precision coulometry is a feasible measurement to detect the onset of Li plating (Figure 9a).[133] As mentioned before, parts of plated metallic Li can re-insert into the graphite or be stripped when discharging, which can induce a rise of voltage plateaus during relaxation or discharging process.[150,151] And the appearance of new voltage plateaus in the rest and stripping process can be used to identify the occurrence of Li plating due to the lower potential of metal Li compared with LiC_x. Although some authors reported that the uncertainty of the plateau technique to identify Li plating due to self-heating or new concentration equilibrium rapidly after charging, this kind of method is simple and real-time. And this method of voltage analysis of battery voltage promotes the development of subsequent *in-situ* electrochemical monitoring for Li plating.[152] In addition to direct analysis of voltage curves during resting and discharge, mathematical treatment of voltage or capacity curves (e.g. differential) can also be used for identification of Li plating. As depicted in Figure 7b and Figure 9b, the differential open-circuit voltage analysis (dOCV), differential voltage analysis (DVA), and differential capacity analysis (DCA) are widely utilized to identify the existence of Li plating.[109,150–152] However, smaller discharging current should be applied when uses above methods, because large current can cause higher overpotential which can bring inaccuracy to the analysis of the voltage curve.

In addition, electrochemical impedance spectroscopy (EIS) is another powerful tool to detect Li plating.[153,154] Several reports applying electrochemical impedance spectroscopy (EIS) are available to detect Li plating or study the electrochemical performance of LIBs.[121,154,155] According to previous studies, the curve of impedance data obtained from test without Li deposition would follow a typical U-shaped pattern. However, once Li plating occurred, the shape of the impedance curve deviated its original U-shaped caused by the parallel reaction of Li deposition.[153] Furthermore, two platforms of voltages in the post-charge relaxation profiles could be identified the occurrence of metallic Li deposition (Figure 9c). Besides, the distribution of relaxation times (DRT) analysis is applied in LIBs, which can be used in all cases to well analysis the frequencies during charging and discharging process with accurate identification compared to EIS.[156–159] Therefore, based on the more advanced DRT technology, the development of real-

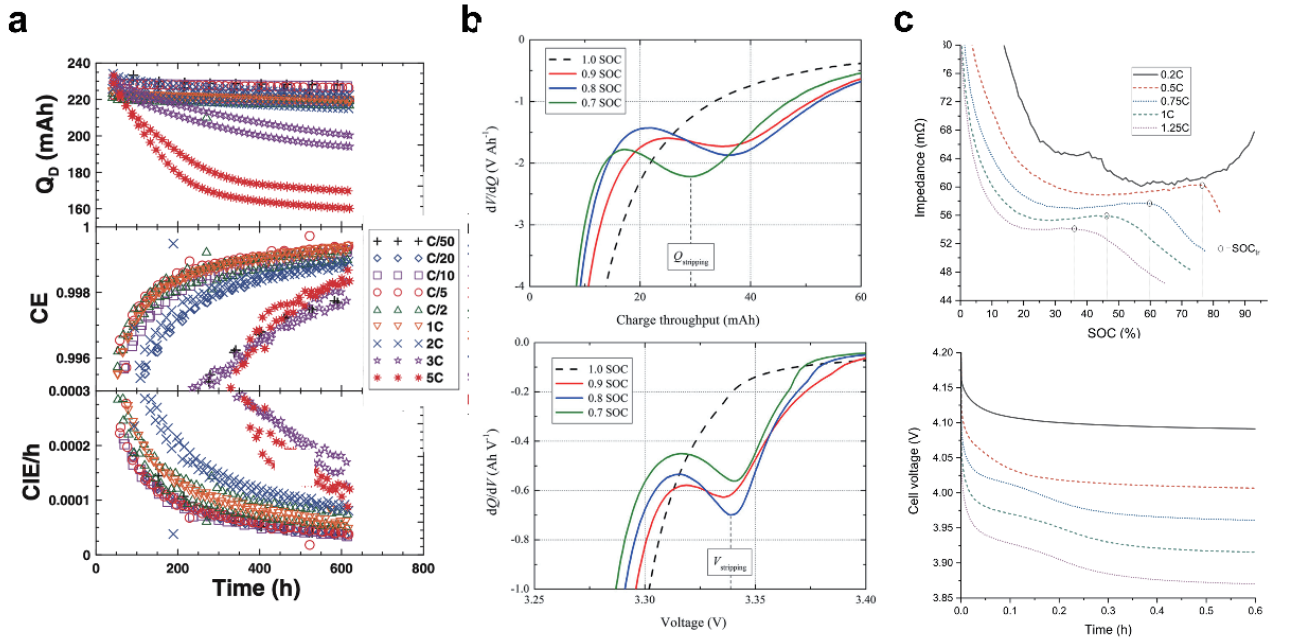

Fig. 9 Li plating detection methods based on different techniques. **a** High precision coulometry.[133] Copyright 2015, IOP Publishing. **b** Differential voltage analysis (DVA), and differential capacity analysis (DCA).[109] Copyright 2014, Elsevier. **c** Electrochemical impedance spectroscopy (EIS) analysis and voltages of post-charge relaxation profiles.[153] Copyright 2020, Elsevier.

DOI: 10.54227/elab.20220011

time detection method can more directly and accurately identify the deposition of Li metal. At the initial node of Li plating, a new electrode/electrolyte interphase is generated by dendrite Li. And the surface capacitance is increased. Through the establishment of equivalent circuit, the surface capacitance measurement technology based on single frequency impedance method is proposed. Therefore, the dynamic capacitance measurement created by Xu et, al. can realize the early warning of Li deposition. Besides, the surface capacitance is linearly correlated with the active surface area, which provides a basis for the quantification of plated Li.[104]

The ultrasonic signals is another potential tool to detect Li plating in commercial LIBs.[160,161] By monitoring the time-of-flight (TOF) shift of acoustic waves, its increment can be used to identify the occurrence of Li metal plating during charging process.[160] Besides, several excellent works have introduced *in-situ* methods to detect plated Li based on neutron and X-ray characterization. The major difference between neutron imaging (radiography and tomography) and X-ray is the matter interacted with sample. The scattering cross sections of X-ray characterization depends on the electron intercalation, while the neutron is determined by nuclear intercalation. To be specific, neutrons are especially sensitive to several elements with low atomic numbers so that Li can be monitored either.[162] It was reported that the neutron radiography is a promising tool to detect plated Li on graphite, which can be verified by direct visualization.[163] In addition to neutron imaging, neutron diffraction (ND) is an powerful technique to investigate the Li deposition behaviour. A commercial 18650 cylindrical cell was monitored by *in-situ* ND to study the relationship of charging-rate and the amount of Li plating and re-insertion of plated Li at −2 °C (Figure 10a).[164] And Zinth et al.[165] investigated the behaviour of Li plating and stripping under different C-rates based on *in-situ* ND at −20 °C (see Figure 10b). As depicted in Figure 10c, neutron depth profiling (NDP) is another useful tool to investigate the sub-surface position of Li atom, and generate concentration depth map of Li.[166,167] Lv et al.[166] employed operando NDP to investigate the spatial heterogeneity of Li during plating and stripping process based on Cu collector, which provides the spatial distribution/density of lithium during plating/stripping.

Unlike the ND measurement, the X-ray diffraction (XRD) can be used to acquire the structural information of different crystalline ingredients based on the X-ray. According to investigating the crystalline peaks of plated Li and other constituents without destruction, *in-situ* XRD can be utilized to detect both local and global Li deposition by focusing small X-ray.

According to investigating the crystalline peaks of plated Li and other constituents without destruction, *in-situ* XRD can be utilized to detect both local and global Li deposition by focusing small X-ray beam. Furthermore, the synchrotron X-ray can give spatial information of metallic Li in short time, which uses the high-energy X-rays. And the spatially resolved XRD has been applied to analyse the process of Li plating behaviour on graphite plane in pouch cell. Figure 11a shows that the plane distribution of Li by using the *in-situ* XRD. By applying the high-energy XRD, the heterogeneity of Li plating during fast charging is obtained directly, who results in accelerating the faster degradation of LIBs.[168] Besides the planar-resolved map of Li deposition, the *operando* depth-resolved XRD has been developed to study the revolution of Li intercalation and plating under high charging rate (Figure 11b). The high speed XRD can capture the spatial and temporal information of the kinetics of graphite electrode during fast charging and discharging in 5 seconds, which demonstrates the remarkable hysteresis between extrusion and intercalation of Li^+.[169] In addition to neutron-based and X-ray-based

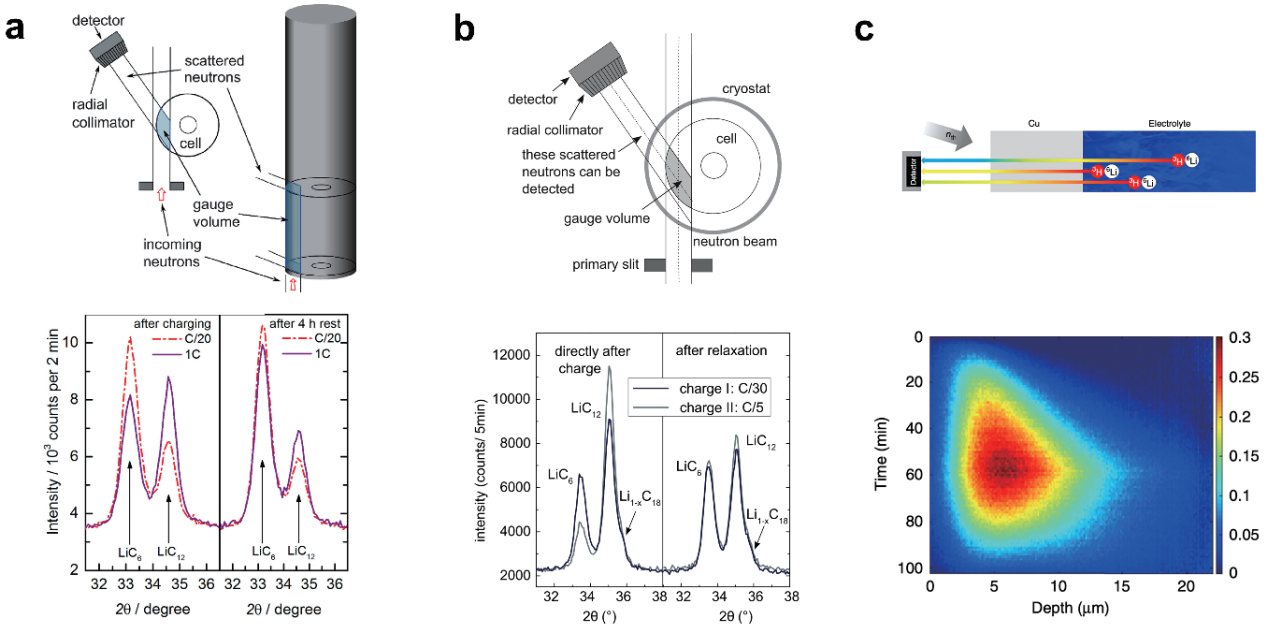

Fig. 10 **a** Raw data of the diffraction reflections of LiC_{12} and LiC_6 by using in-situ neutron diffraction (ND).[164] Copyright 2017, Elsevier. **b** Diffraction data recorded at the beginning and end of this period with the tool of *in-situ* ND.[165] Copyright 2014, Elsevier. **c** The mapping of Li density vs. time from operando neutron depth profiling (NDP) during the first plating and stripping cycle.[166] Copyright 2018, Springer Nature.

DOI: 10.54227/elab.20220011

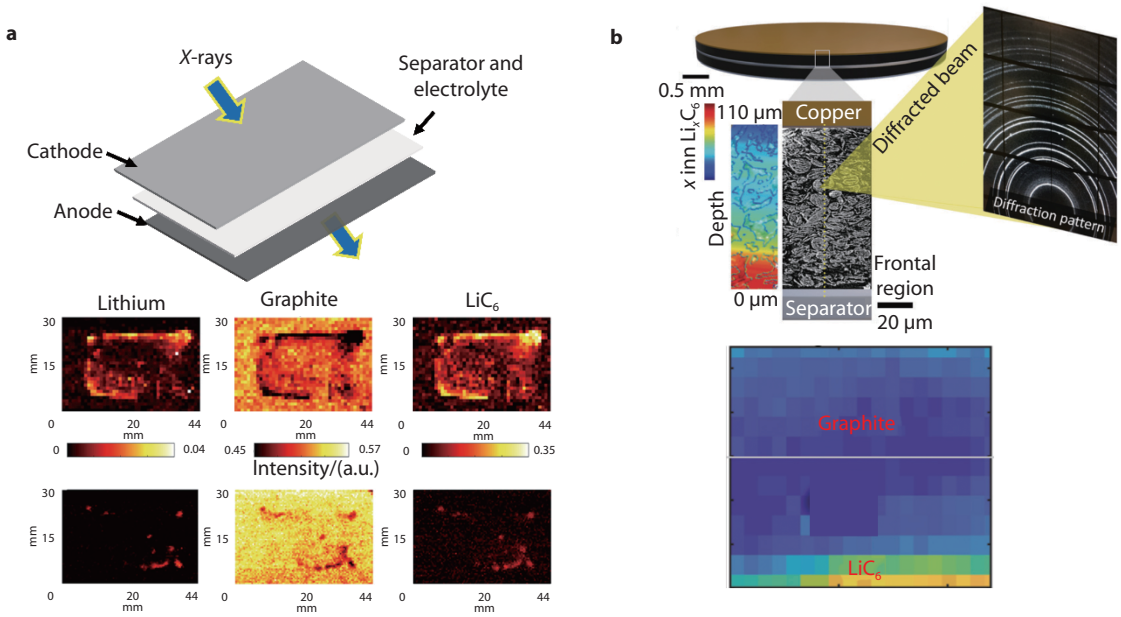

Fig. 11 **a** The Li distribution map over the cross-sectional area of the anode at a particular time (SOC) by using *in-situ* spatially-resolved X-ray diffraction (XRD).[168] Copyright 2020, Elsevier. **b** The *in-situ* depth-resolved XRD to obtain spatial maps of Li over the anode, as a function of time (SOC).[169] Copyright 2020, Royal Society of Chemistry.

monitoring methods, *operando* Raman spectroscopy and *in-situ* optical microscopy are also used to study the process of Li plating onset and re-insertion into graphite in real time.[51,170]

These above detections can indeed accurately and real-time monitor the Li plating onset in LIBs, but in practical applications, such as the power battery pack of EVs, it is difficult to make test equipment miniaturize and portable so that the application of these techniques is limited to the laboratory scale. Hence, it is very vital to find a more simple and accurate method for detecting Li deposition.

ex-situ detection methods

There is no denying that most of *ex-situ* techniques investigating Li plating need the post-mortem graphite electrodes after cycling. Therefore, characterization of the graphite electrode after work, such as scanning electron microscope (SEM), Raman spectroscopy, transmission electron microscope (TEM), X-ray photoelectron spectra (XPS) and other means, are very common *non-in-situ* monitoring methods.[155,171–173] When metallic Li accumulates at the surface of graphite, it is generally accepted that the electrolyte will react with plated Li to form thicker SEI, which causes the incremental impendence and active Li loss. Furthermore, capacity fade of LIBs will be incurred due to the 2 factors. Thus, the aging trends of LIBs can be used to detect Li plating. And there are a number of practicable approaches to identify the Li plating behaviours such as Arrhenius plot, resistance-capacity plot methods and so on. The aging rate and temperature can be related by Arrhenius equation based on abundant parameters obtained from cycling tests under different temperatures.[31] The aging mechanism of LIBs is divided into two patterns according to temperature. The increasing aging rate for T<25 °C is promoted by Li plating, whereas the degeneration of cathode and SEI growth of anode dominate the aging with rising temperature. As will be described below, there are two modes of aging: (1) Aging mode 1: Li plating, with a faster capacity fade, but lower impendence increment. (2) Aging mode 2: SEI growth, with a slower rate of capacity recession but high rate of resistance rise.[174] And the resistance-capacity plot method (R-Q method) is feasible to identify Li plating after long-term cycling, because plated Li has less influence on the growth rate of impedance due to the higher conductivity of metallic Li compared to SEI. Moreover, as mentioned above, the *in-situ* impedance measurements to investigate Li deposition according to the change of internal resistance is a non-destructive and reliable technique.

As for getting the spatial maps of Li metal, time-of-flight secondary ion mass spectrometry (TOF-SIMS) is a useful tool to generate the mapping of Li distribution on graphite (Figure 12a), while the technique is only utilized in laboratory scale.[108,175,176] Li et al.[108] reported that Li deposition on graphite anode can be induced by transition-metal ions (especially manganese) dissolution from NCM cathode based on TOF-SIMS, and the phenomena could be found even <200 cycles. Moreover, as depicted in Figure 12b, surface enhanced Raman spectroscopy (SERS) is another way to provide spatial mapping of abundant Raman-active materials on graphite electrode, which depends on studying the bands of SEI constituents who is enhanced by adjacent metallic Li. And the SERS was used to detect the inhomogeneous Li deposition under high rate due to the interaction between metallic Li nuclei and SEI forming an acetylide species (Li_2C_2).[177]

There is thereby an urgent need but it is still a significant challenge to precisely quantified the amount of plated Li. Son et al.[178] used inductively coupled plasma mass spectroscopy (ICP-MS) to quantified the deposited Li based on NMC532/graphite cell during 6 C charging rate, who showed the Li plating reached 25.59 μmole by the 100th cycle. Otherwise, TGC (short for titration gas chromatography) as a quantitative detection has been developed into a highly sensitive

DOI: 10.54227/elab.20220011

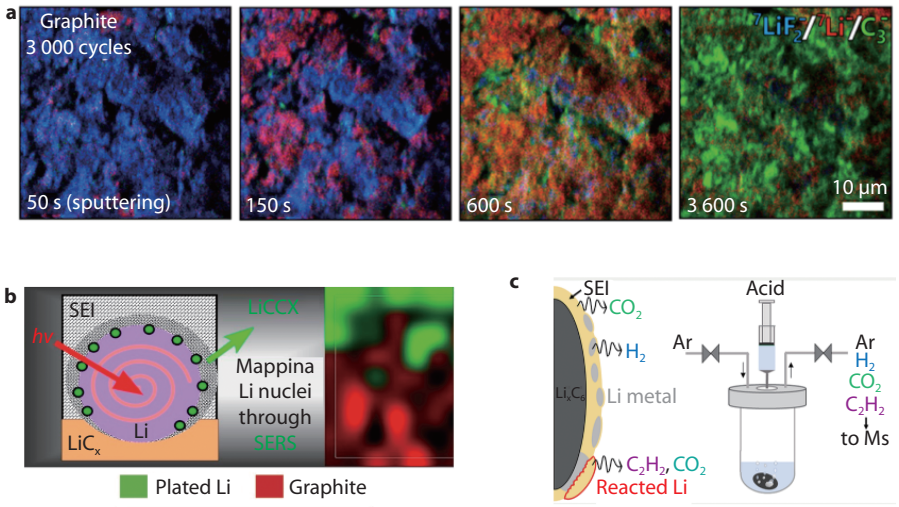

Fig. 12 **a** Spatial maps from a graphite anode over cycling as a function of the sputtering depth by using time-of-flight secondary ion mass spectrometry (TOF-SIMS).[108] Copyright 2017, American Chemical Society. **b** Spatial maps from surface enhanced Raman spectroscopy (SERS) using Raman-active Li_2C_2.[177] Copyright 2019, American Chemical Society. **c** Quantification of inactive Li and SEI species on graphite electrodes after fast charging utilizing titration gas chromatography (TGC).[110] Copyright 2020, American Chemical Society.

tool to quantify inactive Li which still exists on the electrode especially after rapid charging (Figure 12c).[110,179]

As has been emphasized in the article, the plated Li on graphite anode is a hidden danger of fast charging and battery safety. The generation of Li plating contains thermodynamic and kinetic factors, which are discussed in detail in this paper. Therefore, if we want to avoid the deposition of Li on graphite anode, we need to change the electrode and electrolyte and even the charging protocol from the perspective of kinetics and thermodynamics.[180–183] In recent studies, there are two main methods to prevent Li plating in the fast charging: one is to optimize the charging algorithm, but this method cannot break the basic limitations caused by the dynamics and transport properties of LIBs. The second is to improve the electrochemical performance of the LIBs by replacing electrolyte, modifying the structure of anode and applying physical field.[184] Herein, it is necessary to introduce the studies of heating batteries for rapid charging, Wang's group achieved many excellent results.[137,185] To be specific, the charging current is first used to rapidly heat the battery at the beginning of charging. And when the temperature of the battery is heated to a predetermined temperature, rapid charging begins. In particular, rapidly preheating LIBs before fast charging can comprehensively improve the dynamic properties and ion transport process of the battery without modifying the battery material. With the fast-charging ability of LIBs improved by heat, the risk of Li deposition has also been greatly reduced.

However, for the practical application of graphite-anode based LIBs, it is difficult to ensure that Li deposition will never occur due to the complex operating conditions, no matter how the electrode and electrolyte developing. In addition, many studies of fast charging highlight the absence of Li plating. Hence, the monitoring of Li plating is very necessary, especially the *operando* detection methods. Once Li plating occurring, however, the functionalized separator which has higher mechanical strength may effectively prevent the dendritic Li from piercing the separator.[186,187] According to per mechanical blocking theory established by Monroe and Newman, Li dendrites can be suppressed if the elastic modulus of the blocking material is 1.8 times higher than that of the metal Li.[188] It is vital for avoiding the internal short circuit of the cathode and anode so that the stability and batteries can be supported.

Conclusions

Since the commercialization of LIBs, we have been conducting researches on it. With the social demand for portable energy, the application scenarios and working conditions of LIBs are very extensive. However, this also leads to increasing chances of battery's abuse and harsh work, which is a great challenge to stability and safety of LIBs. We know a lot about LIBs, but it is far enough for a perfect battery due to the additional mysteries that we do not know. For instance, Li plating on graphite anode is the major factors which restricts fast charging and triggers safety issues as well as degradation of LIBs. Therefore, solving the problem of Li plating in batteries will benefit the research and development of high safety and high performance of LIBs. However, no definite conclusion has been reached about the mechanism and influencing factors of Li plating.

To gains more insight about Li plating, this article extends the knowledge between the structure as well as interface chemistry of graphite which play a crucial role in Li intercalation and plating.

In the current study, it is well accepted that the SEI formed on graphite is critical for the process of Li intercalation, plating, and deintercalation. Hence, the SEI formation, composition and structure should be studied in detail. During SEI formation, the process of Li^+ inserted into graphite is also taking place. The 4 stags of intercalation process are introduced in detail, and furtherly, the factors restricting the faster intercalation anility of Li^+ are discussed.

Under some extreme conditions, Li^+ does not inserted into the graphite but directly deposits on the graphite particles, forming metallic Li (Li^0). In order to better analyse the mechanism of Li plating caused by graphite electrode, we briefly

DOI: 10.54227/elab.20220011

reviewed the research on Li intercalation into graphite and Li plating in the past 50 years, and proposed four mechanisms leading to lithium precipitation from a microscopic perspective. It is also pointed out that due to the interaction between dynamics and thermodynamics, the above 4 mechanisms are coupled rather than independent. In addition, the factors leading to the deposition of atomic Li on graphite electrode under different conditions are discussed in detail for the 3-common extreme operating conditions of LIB:

- high state of charge
- high charging rate
- low temperature

Besides, the adverse effects induced by Li plating are reported. Although we have always emphasized that Li plating will lead to the degradation of battery performance and cause safety problems to LIBs, some studies have shown that uniform lithium distribution will be beneficial to improve battery performance and safety. This guides us to think about how to design new battery and charging strategies and even lithium detection methods. The determination of the safe range of lithium chromatography and the intelligent identification of the amount of lithium chromatography will also be a noteworthy aspect in the future. Further, in order to monitor the onset of Li plating or quantify the amount of Li plating, a large number of researchers did excellent jobs for these, and this paper introduces part of these work. Especially the *in-situ* or *operando* techniques about detecting Li plating, it is simpler and more accurate to analyse the original electrochemical data during the cycling of LIBs by various methods. Further mechanistic studies and the development of related tools need to be ongoing studied.

In addition to the above factors and detection methods for Li deposition, the position of Li plating on graphite electrode is also a topic worthy of attention. Once the position of Li plating on the bulk electrode has been determined, optimizing the electrode material to achieve uniform current and electrolyte distribution or optimizing the temperature distribution on the bulk electrode will be effective methods to improve it. Moreover, it is worth doing more to avoid Li plating, which is, for the most part, unfriendly for LIBs performance. Therefore, coating or doping other materials with graphite and optimizing the composition of electrolyte are also effective methods to avoid the occurrence of Li plating on graphite.

AUTHOR CONTRIBUTION

Yi Yang, Lei Xu, and Chong Yan discussed for the layout. Yi Yang wrote the draft, and then Chong Yan, Jia-Qi Huang, and Qiang Zhang edited and polished the paper. All authors had approved the final version.

ACKNOWLEDGEMENTS

This work was supported by National Key Research and Development Program (2021YFB2500300), Beijing Municipal Natural Science Foundation (Z200011), National Natural Science Foundation of China (22109083, 22005172, and 21825501), the Seed Fund of Shanxi Research Institute for Clean Energy (SXKYJF015), Beijing Natural Science Foundation (JQ20004, L182021), and Tsinghua University Initiative Scientific Research Program.

CONFLICT OF INTEREST

The authors declare no conflict of interest.

Received: ((will be filled in by the editorial staff))
Revised: ((will be filled in by the editorial staff))
Published online: ((will be filled in by the editorial staff))

REFERENCES

1. R. M. Dell, *Solid State Ionics*, 2000, 134, 139
2. X.-B. Cheng, R. Zhang, C.-Z. Zhao, Q. Zhang, *Chem. Rev.*, 2017, 117, 10403
3. G. N. Lewis, F. G. Keyes, *J. Am. Chem. Soc.*, 1913, 35, 340
4. M. Whittingham, *Science*, 1976, 192, 1126
5. K. Mizushima, P. C. Jones, P. J. Wiseman, J. B. Goodenough, *Mater. Res. Bull.*, 1980, 15, 783
6. M. Li, J. Lu, Z. Chen, K. Amine, *Adv. Mater.*, 2018, 30, 1800561
7. J. Liu, Z. Bao, Y. Cui, E. J. Dufek, J. B. Goodenough, P. Khalifah, Q. Li, B. Y. Liaw, P. Liu, A. Manthiram, Y. S. Meng, V. R. Subramanian, M. F. Toney, V. V. Viswanathan, M. S. Whittingham, J. Xiao, W. Xu, J. Yang, X.-Q. Yang, J.-G. Zhang, *Nat. Energy*, 2019, 4, 180
8. M. Winter, B. Barnett, K. Xu, *Chem. Rev.*, 2018, 118, 11433
9. C. Yan, R. Xu, Y. Xiao, J. F. Ding, L. Xu, B. Q. Li, J. Q. Huang, *Adv. Funct. Mater.*, 2020, 30, 1909887
10. Y. Yang, C. Yan, J. Q. Huang, *Acta Phys. Chim. Sin.*, 2021, 37, 2010076
11. A. Yoshino, *Angew. Chem., Int. Ed.*, 2012, 51, 5798
12. J. Deng, C. Bae, A. Denlinger, T. Miller, *Joule*, 2020, 4, 511
13. R. Schmuch, R. Wagner, G. Hörpel, T. Placke, M. Winter, *Nat. Energy*, 2018, 3, 267
14. Y. X. Yao, X. Chen, C. Yan, X. Q. Zhang, W. L. Cai, J. Q. Huang, Q. Zhang, *Angew. Chem., Int. Ed.*, 2021, 60, 4090
15. X. Zeng, M. Li, D. Abd El-Hady, W. Alshitari, A. S. Al-Bogami, J. Lu, K. Amine, *Adv. Energy Mater.*, 2019, 9, 1900161
16. Q. Zhao, S. Stalin, C.-Z. Zhao, L. A. Archer, *Nat. Rev. Mater.*, 2020, 5, 229
17. G.-L. Zhu, C.-Z. Zhao, J.-Q. Huang, C. He, J. Zhang, S. Chen, L. Xu, H. Yuan, Q. Zhang, *Small*, 2019, 15, 1805389
18. F. Liao, E. Molin, B. van Wee, *Trans. Rev.*, 2016, 37, 252
19. A. Tomaszewska, Z. Chu, X. Feng, S. O'Kane, X. Liu, J. Chen, C. Ji, E. Endler, R. Li, L. Liu, Y. Li, S. Zheng, S. Vetterlein, M. Gao, J. Du, M. Parkes, M. Ouyang, M. Marinescu, G. Offer, B. Wu, *eTrans.*, 2019, 1, 100011
20. W. Xie, X. Liu, R. He, Y. Li, X. Gao, X. Li, Z. Peng, S. Feng, X. Feng, S. Yang, *J. Energy Storage*, 2020, 32, 101837
21. N. Piao, X. Gao, H. Yang, Z. Guo, G. Hu, H.-M. Cheng, F. Li, *eTrans.*, 2022, 11, 100145
22. X. Han, L. Lu, Y. Zheng, X. Feng, Z. Li, J. Li, M. Ouyang, *eTrans.*, 2019, 1, 100005
23. G. Zhang, X. Wei, S. Chen, J. Zhu, G. Han, H. Dai, *ACS Appl. Energy Mater.*, 2021, 4, 12858
24. T. Ma, S. Wu, F. Wang, J. Lacap, C. Lin, S. Liu, M. Wei, W. Hao, Y. Wang, J. W. Park, *ACS Appl. Mater. Inter.*, 2020, 12, 56086
25. W. Cai, C. Yan, Y.-X. Yao, L. Xu, X.-R. Chen, J.-Q. Huang, Q. Zhang, *Angew. Chem., Int. Ed.*, 2021, 60, 13007
26. W. Cai, Y. X. Yao, G. L. Zhu, C. Yan, L. L. Jiang, C. He, J. Q. Huang, Q. Zhang, *Chem. Soc. Rev.*, 2020, 49, 3806
27. D. Hu, L. Chen, J. Tian, Y. Su, N. Li, G. Chen, Y. Hu, Y. Dou, S. Chen, F. Wu, *Chin. J. Chem.*, 2020, 39, 165
28. Q. Liu, C. Du, B. Shen, P. Zuo, X. Cheng, Y. Ma, G. Yin, Y. Gao, *RSC Adv.*, 2016, 6, 88683
29. T. Waldmann, B.-I. Hogg, M. Wohlfahrt-Mehrens, *J. Power Sources*, 2018, 384, 107
30. T. Waldmann, M. Kasper, M. Wohlfahrt-Mehrens, *Electrochim. Acta*, 2015, 178, 525
31. T. Waldmann, M. Wilka, M. Kasper, M. Fleischhammer, M. Wohlfahrt-Mehrens, *J. Power Sources*, 2014, 262, 129
32. J. Goodenough, K. Park, *J. Am. Chem. Soc.*, 2013, 135, 1167

DOI: 10.54227/elab.20220011

33. M. Winter, J. O. Besenhard, M. E. Spahr, P. Novák, *Adv. Mater.*, 1998, 10, 725
34. A. Yacoby, *Nat. Physics*, 2011, 7, 925
35. H. Yadegari, M. A. Koronfel, K. Wang, D. B. Thornton, I. E. L. Stephens, C. Molteni, P. D. Haynes, M. P. Ryan, *ACS Energy Lett.*, 2021, 6, 1633
36. R. Yazami, P. Touzain, *J. Power Sources*, 1983, 9, 365
37. H. Shi, J. Barker, M. Y. Saïdi, R. Koksbang, L. Morris, *J. Power Sources*, 1997, 68, 291
38. S. Schweidler, L. de Biasi, A. Schiele, P. Hartmann, T. Brezesinski, J. Janek, *J. Phys. Chem. C*, 2018, 122, 8829
39. Z. P. Hu, A. Ignatiev, *Phys. Rev. B*, 1984, 30, 4856
40. M. T. Johnson, H. I. Starnberg, H. P. Hughes, *Surf. Sci.*, 1986, 178, 290
41. M. Jäckle, A. Groß, *J. Chem. Phys.*, 2014, 141, 174710
42. L. Mandeltort, J. T. Yates, *J. Phys. Chem. C*, 2012, 116, 24962
43. D. Fraggedakis, N. Nadkarni, T. Gao, T. Zhou, Y. Zhang, Y. Han, R. M. Stephens, Y. Shao-Horn, M. Z. Bazant, *Energy Environ. Sci.*, 2020, 13, 2142
44. T. Abe, H. Fukuda, Y. Iriyama, Z. Ogumi, *J. Electrochem. Soc.*, 2004, 151, A1120
45. Z. Ogumi, T. Abe, T. Fukutsuka, S. Yamate, Y. Iriyama, *J. Power Sources*, 2004, 127, 72
46. K. Persson, V. A. Sethuraman, L. J. Hardwick, Y. Hinuma, Y. S. Meng, A. van der Ven, V. Srinivasan, R. Kostecki, G. Ceder, *J. Phys. Chem. Lett.*, 2010, 1, 1176
47. K. Xu, *J. Electrochem. Soc.*, 2007, 154, A162
48. K. Xu, A. von Cresce, U. Lee, *Langmuir*, 2010, 26, 11538
49. Y. Yamada, Y. Iriyama, T. Abe, Z. Ogumi, *Langmuir*, 2009, 25, 12766
50. F. Yao, F. Gunes, H. Q. Ta, S. M. Lee, S. J. Chae, K. Y. Sheem, C. S. Cojocaru, S. S. Xie, Y. H. Lee, *J. Am. Chem. Soc.*, 2012, 134, 8646
51. T. Gao, Y. Han, D. Fraggedakis, S. Das, T. Zhou, C.-N. Yeh, S. Xu, W. C. Chueh, J. Li, M. Z. Bazant, *Joule*, 2021, 5, 393
52. M. Li, C. Wang, Z. Chen, K. Xu, J. Lu, *Chem. Rev.*, 2020, 120, 6783
53. L. Zhang, C. Zhu, S. Yu, D. Ge, H. Zhou, *J. Energy Chem.*, 2022, 66, 260
54. E. Peled, *J. Electrochem. Soc.*, 1979, 126, 2047
55. S. J. An, J. Li, C. Daniel, D. Mohanty, S. Nagpure, D. L. Wood, *Carbon*, 2016, 105, 52
56. T. Liu, L. Lin, X. Bi, L. Tian, K. Yang, J. Liu, M. Li, Z. Chen, J. Lu, K. Amine, K. Xu, F. Pan, *Nat. Nanotechnol.*, 2019, 14, 50
57. S. Heiskanen, J. Kim, B. Lucht, *Joule*, 2019, 3, 2322
58. D. M. Seo, D. Chalasani, B. S. Parimalam, R. Kadam, M. Nie, B. L. Lucht, *ECS Electrochem. Lett.*, 2014, 3, A91
59. B. Subramanian Parimalam, A. MacIntosh, R. Kadam, B. Lucht, *J. Phys. Chem. C*, 2017, 121, 22733
60. L. Wang, A. Menakath, F. Han, Y. Wang, P. Y. Zavalij, K. J. Gaskell, O. Borodin, D. Iuga, S. P. Brown, C. Wang, K. Xu, B. W. Eichhorn, *Nat. Chem.*, 2019, 11, 789
61. J. Kim, J. G. Lee, H.-s. Kim, T. J. Lee, H. Park, J. H. Ryu, S. M. Oh, *J. Electrochem. Soc.*, 2017, 164, A2418
62. C. Wang, L. Xing, J. Vatamanu, Z. Chen, G. Lan, W. Li, K. Xu, *Nat. Commun.*, 2019, 10, 3423
63. M. Gauthier, T. Carney, A. Grimaud, L. Giordano, N. Pour, H.-H. Chang, D. Fenning, S. Lux, O. Paschos, C. Bauer, F. Maglia, S. Lupart, P. Lamp, Y. Shao-Horn, *J. Phys. Chem. Lett.*, 2015, 6, 4653
64. A. N. Dey, *Thin Solid Films*, 1977, 43, 131
65. E. Peled, D. Golodnitsky, G. Ardel, *J. Electrochem. Soc.*, 1997, 144, L208
66. D. Aurbach, *J. Power Sources*, 2000, 89, 206
67. D. Chen, M. Mahmoud, J.-H. Wang, G. Waller, B. Zhao, C. Qu, M. ElSayed, M. Liu, *Nano Lett.*, 2019, 19, 2037
68. S. Jurng, Z. L. Brown, J. Kim, B. L. Lucht, *Energy Environ. Sci.*, 2018, 11, 2600
69. Y. Zhou, M. Su, X. Yu, Y. Zhang, J.-G. Wang, X. Ren, R. Cao, W. Xu, D. R. Baer, Y. Du, O. Borodin, Y. Wang, X.-L. Wang, K. Xu, Z. Xu, C. Wang, Z. Zhu, *Nat. Nanotechnol.*, 2020, 15, 224
70. C. Hou, J. Han, P. Liu, C. Yang, G. Huang, T. Fujita, A. Hirata, M. Chen, *Adv. Energy Mater.*, 2019, 9, 1902675
71. W. Huang, P. Attia, H. Wang, S. Renfrew, N. Jin, S. Das, Z. Zhang, D. Boyle, Y. Li, M. Bazant, B. McCloskey, W. Chueh, Y. Cui, *Nano Lett.*, 2019, 19, 5140
72. C. Yan, L. Haoran, C. Xiang, X.-Q. Zhang, X.-B. Cheng, R. Xu, J.-Q. Huang, Q. Zhang, *J. Am. Chem. Soc.*, 2019, 141, 9422
73. C. Yan, H. Yuan, H. S. Park, J.-Q. Huang, *J. Energy Chem.*, 2020, 47, 217
74. W. Li, H. Li, *J. Energy Chem.*, 2020, 45, 126
75. O. Borodin, X. Ren, J. Vatamanu, A. Cresce, J. Knap, K. Xu, *Acc. Chem. Res.*, 2017, 50, 2886
76. Z. Liu, *Acta Phys. Chim. Sin.*, 2019, 35, 1293
77. L. L. Zhang, X. S. Zhao, *Chem. Soc. Rev.*, 2009, 38, 2520
78. A. Cresce, M. Gobet, O. Borodin, J. Peng, S. Russell, E. Wikner, A. Fu, L. Hu, H.-S. Lee, Z. Zhang, X.-Q. Yang, S. Greenbaum, K. Amine, K. Xu, *J. Phys. Chem. C*, 2015, 119, 27255
79. A. von Cresce, K. Xu, *Electrochem. Solid State Lett.*, 2011, 14, A154
80. K. Xu, A. von Wald Cresce, *J. Mater. Res.*, 2012, 27, 2327
81. T. Abe, M. Ohtsuka, F. Sagane, Y. Iriyama, Z. Ogumi, *J. Electrochem. Soc.*, 2004, 151, A1950
82. R. Xu, J.-F. Ding, X.-X. Ma, C. Yan, Y.-X. Yao, J.-Q. Huang, *Adv. Mater.*, 2021, 33, 2105962
83. Y. Yamada, K. Furukawa, K. Sodeyama, K. Kikuchi, M. Yaegashi, Y. Tateyama, A. Yamada, *J. Am. Chem. Soc.*, 2014, 136, 5039
84. Y. Yamada, J. Wang, S. Ko, E. Watanabe, A. Yamada, *Nat. Energy*, 2019, 4, 269
85. Y. Yamada, M. Yaegashi, T. Abe, A. Yamada, *Chem. Commun.*, 2013, 49, 11194
86. X.-Q. Zhang, X. Chen, X.-B. Cheng, B.-Q. Li, X. Shen, C. Yan, J.-Q. Huang, Q. Zhang, *Angew. Chem., Int. Ed.*, 2018, 57, 5301
87. Y.-X. Yao, X. Chen, C. Yan, X.-Q. Zhang, W.-L. Cai, J.-Q. Huang, Q. Zhang, *Angew. Chem., Int. Ed.*, 2021, 60, 4090
88. K. Xu, Y. Lam, S. Zhang, R. Jow, T. Curtis, *J. Phys. Chem. C*, 2007, 111, 7411
89. T. R. Jow, M. B. Marx, J. L. Allen, *J. Electrochem. Soc.*, 2012, 159, A604
90. I. Yamada, Y. Iriyama, T. Abe, Z. Ogumi, *J. Power Sources*, 2007, 172, 933
91. I. Yamada, K. Miyazaki, T. Fukutsuka, Y. Iriyama, T. Abe, Z. Ogumi, *J. Power Sources*, 2015, 294, 460
92. K. J. Griffith, K. M. Wiaderek, G. Cibin, L. E. Marbella, C. P. Grey, *Nature*, 2018, 559, 556
93. Y. Xia, T. S. Mathis, M.-Q. Zhao, B. Anasori, A. Dang, Z. Zhou, H. Cho, Y. Gogotsi, S. Yang, *Nature*, 2018, 557, 409
94. X. Xie, Y. Li, Z.-Q. Liu, M. Haruta, W. Shen, *Nature*, 2009, 458, 746
95. A. N. Dey, B. P. Sullivan, *J. Electrochem. Soc.*, 1970, 117, 222
96. P. Arora, M. Doyle, R. E. White, *J. Electrochem. Soc.*, 1999, 146, 3543
97. C. K. Huang, J. S. Sakamoto, J. Wolfenstine, S. Surampudi, *J. Electrochem. Soc.*, 2000, 147, 2893
98. B. K. Purushothaman, U. Landau, *J. Electrochem. Soc.*, 2006, 153, A533
99. S. S. Zhang, K. Xu, T. R. Jow, *J. Power Sources*, 2006, 160, 1349
100. N. Legrand, B. Knosp, P. Desprez, F. Lapicque, S. Raël, *J. Power Sources*, 2014, 245, 208
101. J. Duan, Y. Zheng, W. Luo, W. Wu, T. Wang, Y. Xie, S. Li, J. Li, Y. Huang, *Natl. Sci. Rev.*, 2020, 7, 1208
102. X. M. Liu, C. B. Arnold, *J. Electrochem. Soc.* , 2020, 167, 130519
103. H. Wang, Y. Zhu, S. C. Kim, A. Pei, Y. Li, D. T. Boyle, H. Wang, Z. Zhang, Y. Ye, W. Huang, Y. Liu, J. Xu, J. Li, F. Liu, Y. Cui, *Proc. Natl. Acad. Sci. U. S. A.*, 2020, 117, 29453
104. L. Xu, Y. Xiao, Y. Yang, S. J. Yang, X. R. Chen, R. Xu, Y. X. Yao, W. L. Cai, C. Yan, J. Q. Huang, Q. Zhang, *Angew. Chem., Int. Ed.*, 2022, 61, e202210365
105. P. Bai, J. Li, F. R. Brushett, M. Z. Bazant, *Energy Environ. Sci.*, 2016, 9, 3221
106. H. Ge, T. Aoki, N. Ikeda, S. Suga, T. Isobe, Z. Li, Y. Tabuchi, J. Zhang, *J. Electrochem. Soc.*, 2017, 164, A1050
107. S. S. Zhang, K. Xu, T. R. Jow, *J. Power Sources*, 2003, 115, 137
108. W. Li, U. H. Kim, A. Dolocan, Y. K. Sun, A. Manthiram, *ACS Nano*,

DOI: 10.54227/elab.20220011

2017, 11, 5853
109. M. Petzl, M. A. Danzer, *J. Power Sources*, 2014, 254, 80
110. E. J. McShane, A. M. Colclasure, D. E. Brown, Z. M. Konz, K. Smith, B. D. McCloskey, *ACS Energy Lett.*, 2020, 5, 2045
111. S. S. Zhang, *InfoMat*, 2021, 3, 125
112. K.-E. Kim, J. Y. Jang, I. Park, M.-H. Woo, M.-H. Jeong, W. C. Shin, M. Ue, N.-S. Choi, *Electrochem. Commun.*, 2015, 61, 121
113. Z. M. Konz, E. J. McShane, B. D. McCloskey, *ACS Energy Lett.*, 2020, 5, 1750
114. B.-I. Hogg, T. Waldmann, M. Wohlfahrt-Mehrens, *J. Electrochem. Soc.*, 2020, 167, 090525
115. T. Waldmann, B.-I. Hogg, M. Kasper, S. Grolleau, C. G. Couceiro, K. Trad, B. P. Matadi, M. Wohlfahrt-Mehrens, *J. Electrochem. Soc.*, 2016, 163, A1232
116. K. Dokko, N. Nakata, Y. Suzuki, K. Kanamura, *J. Phys. Chem. C*, 2010, 114, 8646
117. M. Angeles Cabañero, J. Altmann, L. Gold, N. Boaretto, J. Müller, S. Hein, J. Zausch, J. Kallo, A. Latz, *Energy*, 2019, 171, 1217
118. Y. Ji, Y. Zhang, C.-Y. Wang, *J. Electrochem. Soc.*, 2013, 160, A636
119. A. Laforgue, X.-Z. Yuan, A. Platt, S. Brueckner, F. Perrin-Sarazin, M. Toupin, J.-Y. Huot, A. Mokrini, *J. Electrochem. Soc.*, 2020, 167, 140521
120. H. p. Lin, D. Chua, M. Salomon, H. C. Shiao, M. Hendrickson, E. Plichta, S. Slane, *Electrochem. Solid State Lett.*, 2001, 4, A71
121. M. Petzl, M. Kasper, M. A. Danzer, *J. Power Sources*, 2015, 275, 799
122. K. Xu, A. Cresce and U. Lee, *Langmuir*, 2010, 26, 11538
123. C. Yan, Y.-X. Yao, W.-L. Cai, L. Xu, S. Kaskel, H. S. Park and J.-Q. Huang, *J. Energy Chem.*, 2020, 49, 335
124. S. S. Zhang, K. Xu, T. R. Jow, *Electrochim. Acta*, 2002, 48, 241
125. R. V. Bugga, M. C. Smart, *ECS Trans.*, 2019, 25, 241
126. J. M. Tarascon, D. Guyomard, *Solid State Ionics*, 1994, 69, 293
127. T. Zhang, E. Paillard, *Front. Chem. Sci. Eng.*, 2018, 12, 577
128. Q. Q. Liu, D. J. Xiong, R. Petibon, C. Y. Du, J. R. Dahn, *J. Electrochem. Soc.*, 2016, 163, A3010
129. K. Xu, *J. Electrochem. Soc.*, 2007, 154, A162
130. G. V. Zhuang, K. Xu, H. Yang, T. R. Jow, P. N. Ross, *J. Phys. Chem. B*, 2005, 109, 17567
131. Y. Ein-Eli, *Electrochem. Solid State Lett.*, 1999, 2, 212
132. A. Yaqub, Y.-J. Lee, M. J. Hwang, S. A. Pervez, U. Farooq, J.-H. Choi, D. Kim, H.-Y. Choi, S.-B. Cho, C.-H. Doh, *J. Mater. Sci.*, 2014, 49, 7707
133. J. C. Burns, D. A. Stevens, J. R. Dahn, *J. Electrochem. Soc.*, 2015, 162, A959
134. N. Ghanbari, T. Waldmann, M. Kasper, P. Axmann, M. Wohlfahrt-Mehrens, *J. Phys. Chem. C*, 2016, 120, 22225
135. A. Iturrondobeitia, F. Aguesse, S. Genies, T. Waldmann, M. Kasper, N. Ghanbari, M. Wohlfahrt-Mehrens, E. Bekaert, *J. Phys. Chem. C*, 2017, 121, 21865
136. B. P. Matadi, S. Geniès, A. Delaille, T. Waldmann, M. Kasper, M. Wohlfahrt-Mehrens, F. Aguesse, E. Bekaert, I. Jiménez-Gordon, L. Daniel, X. Fleury, M. Bardet, J.-F. Martin, Y. Bultel, *J. Electrochem. Soc.*, 2017, 164, A1089
137. X. -G. Yang, T. Liu, Y. Gao, S. Ge, Y. Leng, D. Wang, C.-Y. Wang, *Joule*, 2019, 3, 3002
138. C. Fear, M. Parmananda, V. Kabra, R. Carter, C. T. Love, P. P. Mukherjee, *Energy Storage Mater.*, 2021, 35, 500
139. B. Rieger, S. F. Schuster, S. V. Erhard, P. J. Osswald, A. Rheinfeld, C. Willmann, A. Jossen, *J. Energy Storage*, 2016, 8, 1
140. M. Tang, P. Albertus, J. Newman, *J. Electrochem. Soc.*, 2009, 156, A390
141. Y. Yang, L. Xu, S.-J. Yang, C. Yan, J.-Q. Huang, *J. Energy Chem.*, 2022, 73, 394
142. J. Cannarella, C. B. Arnold, *J. Electrochem. Soc.*, 2015, 162, A1365
143. X.-R. Chen, C. Yan, J.-F. Ding, H.-J. Peng, Q. Zhang, *J. Energy Chem.*, 2021, 62, 289
144. X. Feng, X. He, M. Ouyang, L. Wang, L. Lu, D. Ren, S. Santhanagopalan, *J. Electrochem. Soc.*, 2018, 165, A3748
145. X. Feng, M. Ouyang, X. Liu, L. Lu, Y. Xia, X. He, *Energy Storage Mater.*, 2018, 10, 246
146. P. Jaumaux, J. Wu, D. Shanmukaraj, Y. Wang, D. Zhou, B. Sun, F. Kang, B. Li, M. Armand, G. Wang, *Adv. Funct. Mater.*, 2021, 31, 2008644
147. X. Liu, D. Ren, H. Hsu, X. Feng, G.-L. Xu, M. Zhuang, H. Gao, L. Lu, X. Han, Z. Chu, L. Jianqiu, X. He, K. Amine, M. Ouyang, *Joule*, 2018, 2, 2047
148. D. Ren, X. Feng, L. Lu, M. Ouyang, S. Zheng, J. Li, X. He, *J. Power Sources*, 2017, 364, 328
149. S. Zheng, L. Wang, X. Feng, X. He, *J. Power Sources*, 2018, 378, 527
150. D. Ren, K. Smith, D. Guo, X. Han, X. Feng, L. Lu, M. Ouyang, J. Li, *J. Electrochem. Soc.*, 2018, 165, A2167
151. C. Uhlmann, J. Illig, M. Ender, R. Schuster, E. Ivers-Tiffée, *J. Power Sources*, 2015, 279, 428
152. I. D. Campbell, M. Marzook, M. Marinescu, G. J. Offer, *J. Electrochem. Soc.*, 2019, 166, A725
153. U. R. Koleti, T. Q. Dinh, J. Marco, *J. Power Sources*, 2020, 451, 227798
154. S. Schindler, M. Bauer, M. Petzl, M. A. Danzer, *J. Power Sources*, 2016, 304, 170
155. V. Müller, R.-G. Scurtu, M. Memm, M. A. Danzer, M. Wohlfahrt-Mehrens, *J. Power Sources*, 2019, 440, 227148
156. C. Yan, L.-L. Jiang, Y. Yao, Y. Lu, J.-Q. Huang, Q. Zhang, *Angew. Chem., Int. Ed.*, 2021, 133, 8602
157. J. Illig, M. Ender, T. Chrobak, J. P. Schmidt, D. Klotz, E. Ivers-Tiffée, *J. Electrochem. Soc.*, 2012, 159, A952
158. F. Katzer, M. A. Danzer, *J. Power Sources*, 2021, 503, 230009
159. J. P. Schmidt, P. Berg, M. Schönleber, A. Weber, E. Ivers-Tiffée, *J. Power Sources*, 2013, 221, 70
160. C. Bommier, W. Chang, Y. Lu, J. Yeung, G. Davies, R. Mohr, M. Williams, D. Steingart, *Cell Rep. Phys. Sci.*, 2020, 1, 100035
161. L. Gold, T. Bach, W. Virsik, A. Schmitt, J. Müller, T. E. M. Staab, G. Sextl, *J. Power Sources*, 2017, 343, 536
162. J. B. Siegel, X. Lin, A. G. Stefanopoulou, D. S. Hussey, D. L. Jacobson, D. Gorsich, *J. Electrochem. Soc.*, 2011, 158, A523
163. A. Same, V. Battaglia, H.-Y. Tang, J. W. Park, *J. Appl. Electrochem.*, 2012, 42, 1
164. C. von Lüders, V. Zinth, S. V. Erhard, P. J. Osswald, M. Hofmann, R. Gilles, A. Jossen, *J. Power Sources*, 2017, 342, 17
165. V. Zinth, C. von Lüders, M. Hofmann, J. Hattendorff, I. Buchberger, S. Erhard, J. Rebelo-Kornmeier, A. Jossen, R. Gilles, *J. Power Sources*, 2014, 271, 152
166. S. Lv, T. Verhallen, A. Vasileiadis, F. Ooms, Y. Xu, Z. Li, Z. Li, M. Wagemaker, *Nat. Commun.*, 2018, 9, 2152
167. S. C. Nagpure, R. G. Downing, B. Bhushan, S. S. Babu, L. Cao, *Electrochim. Acta*, 2011, 56, 4735
168. T. R. Tanim, P. P. Paul, V. Thampy, C. Cao, H.-G. Steinrück, J. Nelson Weker, M. F. Toney, E. J. Dufek, M. C. Evans, A. N. Jansen, B. J. Polzin, A. R. Dunlop, S. E. Trask, *Cell Rep. Phys. Sci.*, 2020, 1, 100114
169. D. P. Finegan, A. Quinn, D. S. Wragg, A. M. Colclasure, X. Lu, C. Tan, T. M. M. Heenan, R. Jervis, D. J. L. Brett, S. Das, T. Gao, D. A. Cogswell, M. Z. Bazant, M. Di Michiel, S. Checchia, P. R. Shearing, K. Smith, *Energy Environ. Sci.*, 2020, 13, 2570
170. M. A. Cabañero, M. Hagen, E. Quiroga-González, *Electrochim. Acta*, 2021, 374, 137487
171. D. Belov, M.-H. Yang, *Solid State Ionics*, 2008, 179, 1816
172. C. Hogrefe, S. Hein, T. Waldmann, T. Danner, K. Richter, A. Latz, M. Wohlfahrt-Mehrens, *J. Electrochem. Soc.*, 2020, 167, 140546
173. G. Zhang, X. Wei, G. Han, H. Dai, J. Zhu, X. Wang, X. Tang, J. Ye, *J.*

DOI: 10.54227/elab.20220011

Power Sources, 2021, 484, 229312
174. Y. Zhang, X. Li, L. Su, Z. Li, B. Y. Liaw, J. Zhang, *ECS Trans.*, 2017, 75, 37
175. A. Fedorková, R. Oriňáková, A. Oriňák, A. Heile, H.-D. Wiemhöfer, H. F. Arlinghaus, *Solid State Sciences*, 2011, 13, 824
176. S. Nanda, A. Manthiram, *Energy Environ. Sci.*, 2020, 13, 2501
177. M.-T. Fonseca Rodrigues, V. A. Maroni, D. J. Gosztola, K. P. C. Yao, K. Kalaga, I. A. Shkrob, D. P. Abraham, *ACS Appl. Energy Mater.*, 2019, 2, 873
178. S.-B. Son, D. Robertson, Z. Yang, Y. Tsai, S. Lopykinski, I. Bloom, *J. Electrochem. Soc.*, 2020, 167, 140506
179. C. Fang, J. Li, M. Zhang, Y. Zhang, F. Yang, J. Z. Lee, M.-H. Lee, J. Alvarado, M. A. Schroeder, Y. Yang, B. Lu, N. Williams, M. Ceja, L. Yang, M. Cai, J. Gu, K. Xu, X. Wang, Y. S. Meng, *Nature*, 2019, 572, 511
180. J. Lu, Z. Chen, F. Pan, Y. Cui, K. Amine, *Electrochem. Energy Rev.*, 2018, 1, 35
181. J. Han, W. Wei, C. Zhang, Y. Tao, W. Lv, G. Ling, F. Kang, Q.-H. Yang, *Electrochem. Energy Rev.*, 2018, 1, 139
182. Y. Ding, Z. P. Cano, A. Yu, J. Lu, Z. Chen, *Electrochem. Energy Rev.*, 2019, 2, 1
183. X. Liu, T. Ji, H. Guo, H. Wang, J. Li, H. Liu, Z. Shen, *Electrochem. Energy Rev.*, 2022, 5, 401
184. T. Liu, X.-G. Yang, S. Ge, Y. Leng, C.-Y. Wang, *eTrans.*, 2021, 7, 100103
185. X.-G. Yang, T. Liu, C.-Y. Wang, *Nat. Energy*, 2021, 6, 176
186. R.-M. Gao, H. Yang, C.-Y. Wang, H. Ye, F.-F. Cao, Z.-P. Guo, *Angew. Chem., Int. Ed.*, 2021, 60, 25508
187. Z. Wang, Y. Wang, C. Wu, W. K. Pang, J. Mao, Z. Guo, *Chem. Sci.*, 2021, 12, 8945
188. H. Hao, T. Hutter, B. L. Boyce, J. Watt, P. Liu, D. Mitlin, *Chem. Rev.*, 2022, 122, 8053

©2022 The Authors. *Energy Lab* is published by Lab Academic Press. This is an open access article under the terms of the Creative Commons Attribution License, which permits use, distribution and reproduction in any medium, provided the original work is properly cited.

Biographies

Yi Yang received his B.E. degree from Sun Yue-Qi Honors College in China University of Mining and Technology (2020). Presently, he is a Ph.D. student in Advanced Research Institute of Multidisciplinary Science (ARIMS), Beijing Institute of Technology, under the supervision of Prof. Jia-Qi Huang. His current research interests focus on the fast charging and the Li plating issue of graphite anode.

Lei Xu received his B.E. degree in Chemical Engineering from Beijing Institute of Technology in 2018. Then, he joined Prof. Jia-Qi Huang's group as a Ph.D. student at Advanced Research Institute of Multidisciplinary Science (ARIMS), Beijing Institute of Technology. His research interest focuses on the interfacial behavior towards fast-charging batteries and the safety of lithium-ion batteries.

Chong Yan received his bachelor's (2013) and master's (2017) degrees from Henan Normal University and got his PhD degrees (2020) at Beijing Institute of Technology. He had done his postdoctoral research at Tsinghua University for two years. He is currently an associate professor in Advanced Research Institute of Multi-disciplinary Science (ARIMS) in Beijing Institute of Technology. His research focuses on the fast-charging technology of lithium-ion batteries and the Nano-sized formation mechanism of electrode/electrolyte interface.

Jia-Qi Huang received his BEng (2007) and PhD (2012) degrees in Chemical Engineering from Tsinghua University, China. He is currently a professor in Advanced Research Institute of Multi-disciplinary Science (ARIMS) in Beijing Institute of Technology. His research interests focus on the interface phenomenon and design strategies for high-energy density rechargeable batteries, including Li–S batteries, Li metal batteries, etc.

Qiang Zhang received his bachelor's and PhD degrees from Tsinghua University in 2004 and 2009, respectively. After spending some time at Case Western Reserve University, USA, and Fritz Haber Institute of the Max Planck Society, Germany, he was appointed as a faculty member at Tsinghua University in 2011. His interests are focused on energy materials, including Li–S batteries, Li metal anode, 3D graphene, and electro-catalysts. He was awarded The National Science Fund for Distinguished Young Scholars, Young Top-Notch Talent from China, and Newton Advanced Fellowship from the Royal Society, UK. Currently, he is an associate editor of the Journal of Energy Chemistry and Energy Storage Materials.